European Journal of Wood and Wood Products (2026) 84:57
https://doi.org/10.1007/s00107-026-02406-4

ORIGINAL ARTICLE

# Green flame retardancy: biomass-based treatment for poplar wood

Igor Wachter[1] · Veronika Kvorková[1] · Tomáš Štefko[1] · Peter Rantuch[1] · Jozef Martinka[1] · Chia-Feng Lin[2] · Lenka Blinová[1]

Received: 10 December 2025 / Accepted: 6 March 2026


**Abstract**

Poplar wood (*Populus alba* L.) was modified using a fully bio-based flame-retardant system based on furfuryl alcohol (FA) and ammonium phytate (AMP), catalysed by phosphoric acid ($H_3PO_4$). The treatment enables in-situ polymerization of FA to form a cross-linked poly(furfuryl alcohol) (PFA) network that immobilizes the nitrogen-phosphorus flame retardant within the wood structure. The modified wood exhibited a weight% gain of ≈22% and a density increase from 0.39 to 0.50 g $cm^{-3}$. FTIR and SEM–EDX confirmed incorporation of phosphorus- and nitrogen-containing species throughout the wood matrix. Fire testing showed a substantial improvement in flame retardancy, including an increase in limiting oxygen index from 18% to 28%, a strong reduction in heat release and smoke production, and a more than six-fold increase in residual char. Thermogravimetric analysis demonstrated earlier dehydration and enhanced char formation, consistent with a synergistic condensed-phase mechanism of the P–N system. Importantly, the treatment exhibited high leach resistance (>90%), and the enhanced fire performance was largely retained after a 14-day leaching procedure, confirming durable fixation of the flame-retardant components. The combined FA+AMP+$H_3PO_4$ system also reduced water uptake and improved surface hardness, while maintaining acceptable mechanical performance. The results demonstrate that phosphoric acid can act as a dual-function catalyst and supplementary phosphorus source, enabling a low-concentration, renewable, and durable flame-retardant modification of fast-growing poplar wood. This approach provides a sustainable pathway for producing multifunctional, high-performance lignocellulosic materials.

## 1 Introduction

Wood, a renewable lignocellulosic biomass, is a promising alternative to fossil-based materials. With an exceptional strength-to-weight ratio and the ability to sequester carbon, it's a valuable material for construction and decorative applications (Sangregorio et al. 2020; Zhang et al. 2021). The rapid growth of poplar makes it an especially attractive resource. However, its inherent flammability remains a major limitation and improving its performance through chemical modification is crucial for expanding its applications.

Chemical modification alters wood properties by changing the composition of its cell walls or modifying its structure (Rowell 1983).

Wood is naturally rich in hydroxyl groups originating from cellulose and hemicelluloses, which strongly influence its hygroscopicity and thermal degradation behaviour. These hydroxyl groups make wood prone to swelling and shrinking with changes in moisture and also contribute significantly to its flammability (Jones et al. 2020; Dong et al. 2023). During heating, the dehydration and depolymerization of these hydroxyl-rich polysaccharides generate flammable volatiles that sustain combustion. Consequently, chemical modification strategies often aim to reduce the accessibility of hydroxyl groups and alter these degradation pathways (Hill 2006). However, while processes like furfurylation effectively reduce hygroscopicity and increase hydrophobicity, they do not inherently suppress heat release or smoke formation, necessitating additional flame-retardant functionality (Rantuch et al. 2024).

✉ Tomáš Štefko
tomas.stefko@stuba.sk

[1] Institute of Integrated Safety, Faculty of Materials Science and Technology in Trnava, Slovak University of Technology in Bratislava, Trnava 91724, Slovakia

[2] Department of Engineering Sciences and Mathematics, Wood Science and Engineering, Luleå University of Technology, Luleå 97187, Sweden

Published online: 13 April 2026

To improve fire safety, wood is commonly treated with flame retardants containing elements such as halogens, phosphorus, nitrogen, or boron through methods like impregnation and coating (Lowden and Hull 2013; Xie et al. 2013). While halogenated compounds are effective, they raise significant environmental and health concerns and are increasingly being phased out (Page et al. 2023). Phosphorus–nitrogen systems are particularly attractive alternatives because they promote condensed-phase char formation and reduce smoke toxicity without relying on halogens.

Phosphorus-based flame retardants are gaining favour due to their lower toxicity and effectiveness in cellulose-based materials (Abou-Okeil et al. 2013). They work primarily by promoting char formation, which slows combustion. A significant challenge, however, is that many flame retardants can leach from the wood, diminishing their long-term effectiveness. This has led to a focus on developing sustainable, bio-based impregnation solutions with high leach resistivity (Lin et al. 2021a, b; Wu et al. 2023).

Phytic acid (PA), a natural phosphorus source, is a promising candidate due to its non-toxicity, low cost, and ability to promote carbonization and scavenge flammable radicals during heating (Cheng et al. 2016; Gao et al. 2019). When combined with nitrogen-rich compounds like urea, it forms ammonium phytate (AMP), which offers a powerful synergistic flame-retardant effect. In this system, phosphorus promotes char formation while nitrogen produces non-combustible gases (Song et al. 2022; Li et al. 2022, 2024a; Qin et al. 2023).

The issue of leaching from these small-molecule flame retardants can be solved by embedding them within a polymerized resin matrix. Furfuryl alcohol (FA) is an environmentally friendly chemical derived from agricultural biomass (Yao et al. 2017). Its water-soluble nature allows it to penetrate wood cell walls, where it polymerizes in-situ into poly(furfuryl alcohol) (PFA). This improves the wood's dimensional stability and resistance to biodegradation (Ehmcke et al. 2020). However, PFA itself can contribute to flame spread and toxic smoke release during combustion (Gaefke et al. 2007; Zhang et al. 2020).

Previous studies have explored combining these approaches. Liangliang Zhang et al., (2022) used a boron/phosphorus system to catalyse FA polymerization while providing fire resistance. Similarly, in other research the fire performance of pine wood with an ammonium phytate-based flame retardant was improved (Zhang et al. 2023). More recently, a study by (Xie et al. 2024) demonstrated that the in-situ polymerization of FA and ammonium phytate (AMP) could enhance flame retardancy, dimensional stability, and leach resistance. However, these approaches often require high chemical loadings or catalysts that function solely as curing agents without contributing to flame retardancy. These limitations highlight the need for a low-concentration, highly efficient furfurylated wood system that integrates heat insulation, smoke suppression, and durable flame-retardant functionality.

To address these limitations, this study proposes a novel, fully bio-based modification system. Unlike previous approaches that may use volatile acids or high concentrations of AMP, this work introduces the use of phosphoric acid ($H_3PO_4$) as a dual-function agent.

First, it acts as an efficient catalyst for the in-situ polymerization of FA at low concentrations (Origo et al. 2016). In addition to catalysing furfuryl alcohol polymerization, phosphoric acid can influence the structure of the resulting poly(furfuryl alcohol) network by promoting dehydration and condensation reactions that increase crosslink density (Choura et al. 1996).

Second, the non-volatile phosphoric acid is expected to remain within the wood matrix and act as a supplementary phosphorus source, which may synergize with AMP to promote dehydration and char formation (Hörold 2014; Zhang et al. 2022b). This dual-function concept distinguishes the present approach from FA+AMP systems in which the catalyst is used solely to initiate FA polymerization.

Therefore, the objective of this work was to develop and validate a "green", low-concentration, fully bio-based, renewable, and low toxicity FA+AMP flame-retardant system for poplar wood, catalysed by $H_3PO_4$ (catalytic amounts) with high durability against leaching, while maintaining acceptable mechanical performance.

This study tests the central hypothesis that the in-situ polymerization of a low-concentration furfuryl alcohol (15 wt%) and ammonium phytate (4 wt%) solution, uniquely catalysed by phosphoric acid, will form a stable, cross-linked matrix that physically entraps the AMP flame retardant. To verify the proposed synergistic mechanism, the modified wood was systematically evaluated by FTIR, SEM–EDX, thermogravimetric analysis, limiting oxygen index, cone calorimetry, and mechanical testing, with direct comparison of performance before and after a 14-day leaching procedure.

The novelty of this work lies in (i) the use of phosphoric acid as a dual-function catalyst and supplementary phosphorus source, (ii) the use of comparatively low concentrations of FA and AMP while still achieving high flame-retardant efficiency, and (iii) the demonstration of retained cone calorimetry performance after leaching, confirming durable fixation of a bio-based nitrogen–phosphorus system.

## 2 Materials and methods

### 2.1 Materials

Poplar wood (*Populus alba* L.) with an average air-dry density of 0.440 ± 0.020 g $cm^{-3}$ was obtained from JAF HOLZ Slovakia, Ltd. (Slovakia). Specimens were cut exclusively from sapwood, free of visible defects. Prior to chemical modification, all samples were oven-dried at 100 °C until both mass and dimensions stabilized. Details regarding the number of replicates, sample sizes, and associated test methods are listed in Table 1.

Phytic acid (PA, $C_6H_{18}O_{24}P_6$, 50 wt% in water), urea ($CH_4N_2O$, 99%), furfuryl alcohol (FA, $C_5H_6O_2$, purity ≥ 98.0%), phosphoric acid ($H_3PO_4$, 85%) was purchased from CENTRALCHEM, Ltd., Slovakia.

### 2.2 Ammonium phytate synthesis

A solution was prepared by dissolving urea (43.2 g, 0.72 mol) and phytic acid (PA) (79.2 g, 0.12 mol) in deionized water (36 g) until fully homogenized. The molar ratio of PA to urea and the synthesis procedure were selected based on previously validated protocols reported in the literature (Feng et al. 2017; Zuo et al. 2023; Qin et al. 2023; Xie et al. 2024),which demonstrated efficient formation of ammonium phytate through acid–base neutralization. The solution was heated in a three-necked flask at 110 °C for 8 h under reflux with continuous stirring to ensure homogeneous heat distribution and complete reaction. After cooling to ambient temperature, a homogeneous, brown-tinted ammonium phytate (AMP) solution with pH ≈ 6 was utilized for the treatment of wood samples.

For the specific preparation of pure AMP for FTIR analysis, a portion of the solution underwent a solvent exchange (performed twice) with anhydrous ethanol at four times the solution volume to precipitate the AMP. The solvent was subsequently decanted, and the obtained AMP was freeze-dried at -55 °C to yield a dry powder suitable for spectroscopic characterization.

### 2.3 Modified poplar wood preparation

Poplar specimens were cut into various dimensions according to standard requirements, and defect-free pieces with an oven-dried density of 0.380 ± 0.020 g $cm^{-3}$ were chosen for modification. The aqueous impregnation solution was formulated by combining 15 wt% FA with 4 wt% AMP, and its pH was adjusted to around 2 using phosphoric acid (approx. concentration of $H_3PO_4$ is 1.6 ml $l^{-1}$)(denoted as FA+AMP-W). The samples were impregnated through the following process: first subjected to a vacuum of 0.3 kPa for 2 h, followed by 16 h of treatment under normal atmospheric pressure. After impregnation, excess solution was removed by wiping with a cloth. The treated specimens were then wrapped in aluminium foil and heat-cured at 130 °C for 24 h to ensure complete reaction of FA and AMP. Subsequent gradual drying was applied until the samples reached a constant weight. For comparison, two sets of control specimens were prepared using the same procedure but with different impregnation solutions: one containing 4 wt% AMP adjusted to pH ≈ 2 with phosphoric acid (AMP-W), and the other containing 15 wt% FA adjusted to pH ≈ 2 (FA-W). Although an additional control consisting of wood treated only with phosphoric acid at pH ≈ 2 was not included, both FA-W and AMP-W control systems were prepared under identical acidic conditions, enabling isolation of the individual contributions of FA and AMP within the phosphoric-acid-catalysed process.

### 2.4 Weight% gain and density

According to Liu et al. (2021), the weight% gain (WPG) of the modified poplar samples was calculated as:

$$WPG\,(\%) = \frac{w_f - w_0}{w_0} \times 100\%$$

**Table 1** Specimen dimensions, number of replicates, and standards used for each test

| Specimen Size ($mm^3$) | Test Type | Replicates ($n$)* | Standard |
|---|---|---|---|
| 100 × 100 × 20 | Cone calorimetry | 24 | ISO 5660-1: 2015 |
| | Leaching | 12 | EN 84 (2020) |
| | Shore D Hardness | 12 | ISO 48−4 (2018) |
| | Janka Hardness | 24 | ASTM D143 (2022) |
| | Colourimetry | 12 | - |
| | Water uptake | 12 | - |
| 20 × 20 × 20 | TGA | 8 | - |
| | FTIR analysis | 4 | - |
| 100 × 10 × 4 | LOI | 40 | ISO 4589-2 (2017) |
| 100 × 20 × 3.5 | Three-point bending test | 24 | ISO 178 (2019) |
| 20 × 20 × 2 | Flame test | 12 | - |

*Replicates refer to the number of specimens tested across all treatments

where $w_0$ is initial weight of oven-dry sample, $w_f$ is the oven-dry weight of sample after impregnation. Additionally, the density was determined according to the GB/T 1927.5–2021 standard. Calculated values of the WPG and densities are shown in Table 3.

## 2.5 Fourier transform infrared spectroscopy

Fourier Transform Infrared (FTIR) spectra were acquired using an Agilent Technologies Varian FT-IR Spectrometer 660 (USA) equipped with a PIKE Technologies GladiATR accessory (USA). Spectra were collected in the 4000–400 $cm^{-1}$ range with a resolution of 2 $cm^{-1}$ and averaged over 256 scans. The final spectra were corrected for background air absorbance. Each sample type (W, AMP-W, FA-W, and FA+AMP-W) was measured at five distinct locations ($n=5$), and the reported spectrum represents the average of these five measurements.

In addition, FTIR spectra of prepared ammonium phytate (AMP), phytic acid, and urea were recorded under the same experimental conditions as reference materials. These reference spectra were used to assist in the identification of characteristic functional groups related to AMP and to support interpretation of nitrogen- and phosphorus-containing bands in the treated wood samples.

## 2.6 Scanning electron microscopy

The morphology of the samples was observed with high resolution scanning electron microscope JEOL JSM 7600 F in secondary electron imaging (LEI). Following parameters were used: U=5 kV, I=2 nA, WD=15 mm. Prior observation, the samples were coated with an amorphous carbon (10–20 nm).

Energy-dispersive X-ray spectroscopy (EDX) was performed using an EDX detector integrated into the SEM system to determine the elemental composition of the wood samples. EDX spectra were collected for all investigated materials (RW, AMP-W, FA-W, and FA+AMP-W) from representative cross-sectional regions. Particular attention was given to the detection of phosphorus (P), as a key element originating from the ammonium phytate/phosphoric acid flame-retardant system. The obtained spectra were used for qualitative and semi-quantitative comparison of elemental presence among the different treatments.

In addition, elemental mapping was conducted for the FA+AMP-W sample to visualize the spatial distribution of the main elements within the treated wood structure. Mapping was performed on a representative cross-sectional area containing both cell wall and lumen regions. Elemental maps were acquired for carbon (C), oxygen (O), and phosphorus (P), confirming the presence and distribution of phosphorus within the wood matrix after the combined FA+AMP treatment.

## 2.7 Colourimetry

Colour measurements were performed with a NR200 Precision Colorimeter (Threenh Technology Co., Ltd., Shenzhen, China) using an Φ8 mm aperture, CIE L**a**b* colour space, and D65 light source. Each test specimen was measured 5 times, and the colour change from raw sample was calculated from:

$$\Delta E_t = \sqrt{(L_1 - L_0)^2 + (a_1 - a_0)^2 + (b_1 - b_0)^2}$$

where $\Delta E_t$ is the total colour difference at time $t$; $_1$ is the value of coordinate indicating lightness after the test; $_0$ is the initial value of coordinate indicating lightness, $a_1$ is the value of coordinate position between red and green after the test; $a_0$ is the initial value of coordinate position between red and green; $b_1$ is the value of coordinate position between yellow and blue after the test; $b_0$ is the initial value of coordinate position between yellow and blue.

## 2.8 Flexural strength

Flexural properties were determined by three-point bending using a UMZ-3k universal testing machine equipped with an SZ-3000 displacement sensor (Micro-Epsilon, Czechia). The measurements were carried out in accordance with ISO EN 178. Rectangular specimens with dimensions of 100 mm × 20 mm × 3.5 mm (length × width × thickness) were tested using a support span of 80 mm. Loading was applied at a constant crosshead speed of 2 $mm \cdot s^{-1}$ until failure. The applied load and mid-span displacement were continuously recorded.

The modulus of rupture (MOR) was calculated using:

$$MOR = \frac{3F_{max}L}{2bh^2}$$

where $F_{max}$ is the maximum load (N), L is the support span (mm), b is the specimen width (mm), and h is the specimen thickness (mm).

The modulus of elasticity (MOE) was calculated from the slope of the initial linear region of the load–displacement curve:

$$MOE = \frac{L^3 m}{4bh^3}$$

where m is the slope of the load–displacement curve (N $mm^{-1}$), and L, B, and h are defined as above.

### 2.9 Hardness

To evaluate the hardness of the modified poplar wood samples, two distinct methods were employed. Shore D hardness was assessed using a Sauter HD Digital Shore D Hardness Tester (Sauter GmbH, Balingen, Germany), in accordance with the Shore Hardness Test ISO 48−4 (ASTM D2240) standard. Additionally, Janka hardness was measured according to ASTM D143. For both measurements, the hardness was tested perpendicular to the grain of the samples to ensure consistent and accurate data collection.

### 2.10 Leaching test and water uptake

Leaching tests were performed in three replicates according to EN 84 (2020), with specimens' vacuum-treated for 20 min and leached in water replaced ten times over 14 days. After this period, the surface of the samples was dried, and the samples were weighed to determine the water uptake, according to the equation:

$$WU = \frac{m_{wu} - m_1}{m_1} \times 100\%$$

where WU is water uptake (%); $m_1$ is the weight of the dry-oven sample after the corresponding solution impregnation (g); $m_{wu}$ is wet weight of the sample after leaching test (g).

Subsequently, the leached specimens were oven-dried at 103 °C, before measuring the dry mass. In this experiment the leach retention (LR; the weight of impregnation substance retained in the sample after leaching test) was calculated from:

$$LR = \left(1 - \frac{m_1 - m_f}{m_1 - m_0}\right) \times 100\%$$

where LR is leach retention (%); $m_1$ is the weight of the dry-oven sample after the corresponding solution impregnation (g); $m_0$ is initial the dry-oven weight of the sample (g); $m_f$ is the weight of dry oven sample after the leaching test.

### 2.11 Thermogravimetric analysis

Thermogravimetric analysis (TGA) analysis was performed to assess the thermal degradation of various wood samples. The study included raw wood (RW), furfuryl alcohol-treated wood (FA-W), AMP-treated wood (AMP-W), and wood treated with both furfuryl alcohol and AMP (FA+AMP-W). Measurements were taken on samples before and after a leaching process.

Measurements were performed using a Netsch STA 449 F5 Jupiter instrument. Each sample was prepared by crushing and drying at 103 °C to a constant weight, with a final weight of approximately 5 mg. The analysis was carried out under a inert ($N_2$) atmosphere (60 mL/min) with a heating rate of 10 °C/min, from 35 °C to 800 °C.

### 2.12 Fire performance test

The fire hazards of the materials were determined using a cone calorimeter, following the ISO 5660-1:2015 standard (International Organization for Standardization 2015). This standard specifies the procedure for assessing the heat release rate, smoke production, and mass loss rate of materials.

Samples were exposed to an external radiant heat flux of 50 ± 0.5 kW $m^{-2}$. Three individual replicates of each material type (RW, AMP-W, FA-W, and FA+AMP-W) were tested for their fire performance. The measurements were conducted both before and after a leaching procedure to evaluate the durability of the fire performance properties.

For each material, four replicate measurements were used to calculate sample densities. These values, along with the ambient measurement conditions, are presented in Table 2.

### 2.13 Limiting oxygen index

The Limiting Oxygen Index (LOI) test was conducted to evaluate the flammability of the samples. This standard method determines the minimum concentration of oxygen, expressed as a percentage, required in a mixture with nitrogen to support the sustained combustion of a material. The LOI tests were performed in accordance with ISO 4589-2:2017 standards using a customized LOI apparatus (International Organization for Standardization 2017b). Each sample was cut into rectangular specimens measuring 100 mm x 10 mm x 4 mm. The specimens were held vertically in a glass chimney, and a mixture of oxygen and nitrogen was introduced from the bottom. An external flame was used to ignite the top of the specimen. The oxygen concentration was then systematically adjusted to find the minimum value at which the sample continued to burn for at least 3 min, or over a length of 50 mm, after the external flame was removed. This procedure was repeated for each sample type to ensure reproducibility.

### 2.14 Flame test

The flame retardancy of the wood samples was qualitatively assessed using an in-lab direct flame test (Xie et al. 2024).

**Table 2** Density of tested specimens and ambient laboratory conditions during fire performance test (cone calorimetry) for raw wood (RW) and modified wood samples before leaching (NL) and after leaching (L). Values are given as mean ± standard deviation ($n = 3$)

| Sample | Density [g cm$^{-3}$] | Ambient temperature [°C] | Ambient pressure [kPa] | Air humidity [%] |
|---|---|---|---|---|
| RW /NL | 0.384 ± 0.001 | 26.5 ± 0.7 | 100.21 ± 0.28 | 20.00 ± 1.41 |
| RW /L | 0.387 ± 0.008 | 25.3 ± 1.2 | 100.96 ± 1.21 | 23.67 ± 4.62 |
| AMP-W /NL | 0.436 ± 0.022 | 25.0 ± 1.0 | 100.90 ± 1.20 | 24.00 ± 4.36 |
| AMP-W /L | 0.427 ± 0.006 | 24.5 ± 0.7 | 100.32 ± 0.88 | 22.00 ± 3.60 |
| FA-W /NL | 0.475 ± 0.007 | 25.0 ± 1.0 | 100.86 ± 1.23 | 23.67 ± 1.23 |
| FA-W /L | 0.472 ± 0.009 | 25.1 ± 1.2 | 100.85 ± 0.49 | 20.25 ± 1.50 |
| FA + AMP-W /NL | 0.508 ± 0.020 | 24.3 ± 0.6 | 100.24 ± 1.19 | 26.67 ± 4.93 |
| FA + AMP-W /L | 0.480 ± 0.044 | 24.0 ± 1.0 | 100.91 ± 0.87 | 21.30 ± 4.10 |

RW: raw wood; FA-W: furfuryl alcohol-treated wood; AMP-W: ammonium phytate-treated wood; FA + AMP-W: combined treatment; NL: non-leached samples; L: leached samples

**Table 3** Impregnation formulation (wt% in water), weight% gain (WPG) [%], and oven-dry density before ($\rho_0$) and after treatment ($\rho_1$) [g cm$^{-3}$] for raw wood and modified wood samples. Values are reported as mean ± standard deviation ($n = 3$)

| Samples | Impregnation solution | WPG [%] | $\rho_0$ [g cm$^{-3}$] | $\rho_1$ [g cm$^{-3}$] |
|---|---|---|---|---|
| RW | – | – | 0.382 ± 0.019 | – |
| FA-W | 15wt% FA; pH adjusted to ≈2 with $H_3PO_4$ | 20.31 ± 1.74 | 0.364 ± 0.007 | 0.456 ± 0.003 |
| AMP-W | 4wt% AMP; pH adjusted to ≈2 with $H_3PO_4$ | 9.55 ± 0.88 | 0.376 ± 0.009 | 0.417 ± 0.011 |
| FA + AMP-W | 15wt% FA; 4wt% AMP; pH adjusted to ≈2 with $H_3PO_4$ | 21.72 ± 1.61 | 0.394 ± 0.015 | 0.499 ± 0.013 |

RW: raw wood; FA-W: furfuryl alcohol-treated wood; AMP-W: ammonium phytate-treated wood; FA + AMP-W: combined treatment; values are given as mean ± standard deviation ($n = 3$)

Samples were secured in a stainless-steel clamp and positioned 10 cm from the tip of a propane torch. After ignition, the samples were exposed to the flame, and the time required for the flame to burn through the sample was recorded. The flame spread process was documented using a video camera, with simultaneous still photographs taken (0 s, 10 s and after flame-out).

### 2.15 Statistical analysis

Statistical significance of differences in the measured values among the investigated wood modifications was evaluated using Duncan's multiple range test at a significance level of $\alpha = 0.05$. Results of Duncan's test are indicated by letter indexes in the figures. Because listing all Duncan test outcomes for the tables would be excessively long in the main text, the complete pairwise comparison results are provided in Supplementary Material A. Duncan's coefficients were calculated using StatSoft Statistica 10 software.

## 3 Results and discussion

### 3.1 Chemical and physical characterization of unmodified and modified poplar wood

The weight% gain (WPG) and density data in Table 3 demonstrate the effectiveness of the modification process, showing how the uptake of impregnation solutions alters the poplar wood's density. The lowest WPG was achieved in AMP-W samples, namely 9.55 ± 0.88, while the average density of the samples changed from 376 g cm$^{-3}$ to 416 g cm$^{-3}$. WPG of FA-W and FA + AMP-W reached similar. The data suggest that FA and AMP successfully permeated the wood structure, contributing to an enhanced density.

### 3.2 Fourier-transform infrared spectroscopy

To support identification of ammonium phytate-related functional groups in the treated wood, FTIR spectra of phytic acid (PA), urea, and ammonium phytate (AMP) were additionally recorded as reference materials (Fig. 1). The FTIR spectrum of PA exhibited a broad absorption band at 3268 cm$^{-1}$, attributed to O–H stretching vibrations associated with extensive hydrogen bonding. The prominent bands at 1133 and 981 cm$^{-1}$ correspond to phosphate-related vibrations (P = O and P–O–C structures), consistent with previous reports (Xie et al. 2024). In the FTIR spectrum of urea, characteristic absorption bands were observed at 3426 and 3323 cm$^{-1}$, corresponding to asymmetric and symmetric N–H stretching vibrations, respectively. The band at 1676 cm$^{-1}$ was assigned to C = O stretching vibrations, while N–H bending vibrations appeared at 1590 cm$^{-1}$ and the band at 1457 cm$^{-1}$ was attributed to C–N stretching (Grdadolnik and Maréchal 2002). The FTIR spectrum of AMP showed peaks at 1071 and 939 cm$^{-1}$, corresponding to phosphate-related vibrations (P–O and P–O–C stretching modes). In addition, bands at 3219 and 1452 cm$^{-1}$ were

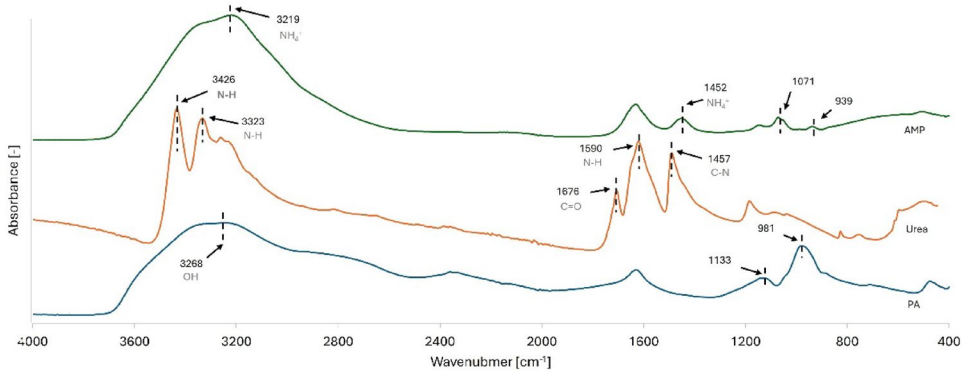


**Fig. 1** FTIR analysis of the phytic acid, urea and synthesised ammonium phytate

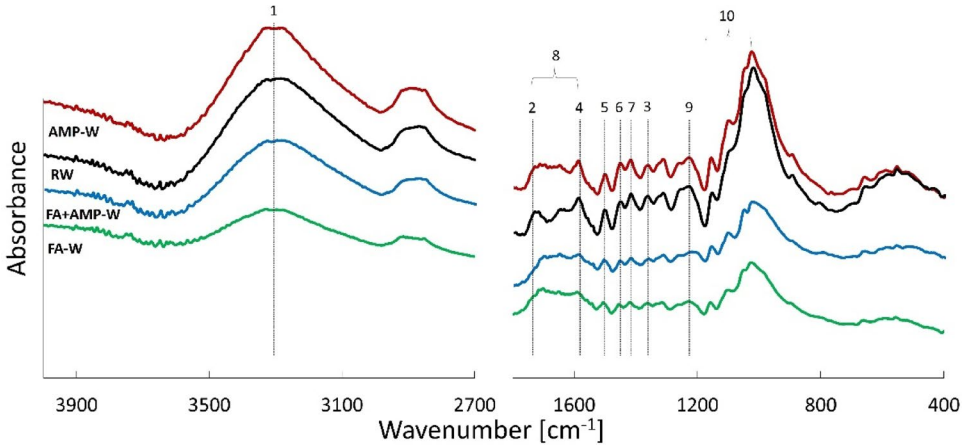


**Fig. 2** FTIR analysis of the raw wood (RW); furfuryl alcohol-treated wood (FA-W); ammonium phytate-treated wood (AMP-W); furfuryl alcohol and ammonium phytate-treated wood (FA+AMP-W)

assigned to $NH_4^+$ ionic vibrations, confirming the formation of ammonium phytate, in agreement with the literature (Xie et al. 2024).

FTIR-ATR spectroscopy was employed to identify the functional groups present in wood and to evaluate the chemical changes resulting from modification (Fig. 2). In the spectrum of unmodified wood (RW), characteristic absorption bands were observed at 3309 $cm^{-1}$, corresponding to O–H stretching vibrations of cellulosic hydroxyl groups (Yang et al. 2022b; Zhang et al. 2022b; Ni et al. 2024; Xie et al. 2024; Brisebois et al. 2025). The band at 1719 $cm^{-1}$ was attributed to unconjugated C=O stretching in xylan, a hemicellulose component (Yang et al. 2022b). Bands at 1591, 1506, and 1421 $cm^{-1}$ corresponded to aromatic skeletal vibrations in lignin (Liu et al. 2022; Zhang et al. 2022b; Ni et al. 2024; Brisebois et al. 2025), while the band at 1451 $cm^{-1}$ represented C–H deformation coupled with aromatic skeletal vibration (Zhang et al. 2022b). Further peaks were detected at 1364 $cm^{-1}$ (C–H deformation in cellulose and hemicellulose) (Zhang et al. 2022b; Brisebois et al. 2025), 1152 $cm^{-1}$ (C–O–C antisymmetric bridge stretching in cellulose and hemicellulose) (Zhang et al. 2022b; Xie et al. 2024), 1102 $cm^{-1}$ (C–O stretching in hemicellulose) (Brisebois et al. 2025), and 1019 $cm^{-1}$ (C–O stretching mainly in cellulose) (Yang et al. 2022a).

Following furfurylation, notable changes were observed in the regions around 3300, 1731, 1589, 1508, 1455, 1419, and 1363 $cm^{-1}$ in the spectra of FA-modified wood (FA-W and FA+AMP-W). The reduced intensity of the O–H band (~3300 $cm^{-1}$) indicates decreased hydroxyl accessibility due to PFA formation within the cell wall (Zhang et al. 2022b). The unconjugated C=O stretching band of xylan shifted slightly to lower wavenumbers (from 1731 to 1700 $cm^{-1}$), accompanied by a decrease in intensity and peak broadening. Such changes are attributed to the incorporation of furfural resin, characterized by a C=O stretching vibration of γ-diketone groups near 1724 $cm^{-1}$ arising from opened furan rings (Yang et al. 2022b; Zhang et al. 2022b). A decrease in the band at 1363 $cm^{-1}$ was also observed, likely resulting from acid hydrolysis of polysaccharides during modification. The reduction in intensity of aromatic skeletal vibration bands at 1589, 1508, 1455, and 1419 $cm^{-1}$ suggests interactions between lignin and furfuryl alcohol during the polycondensation process. These results are consistent with the findings reported by Zhang et al. (2022b). However, due to overlapping contributions in this spectral region, these variations should be interpreted as indicative of structural modification rather than definitive evidence of specific covalent bonding.

After the addition of AMP, further spectral variations were evident in the regions 1510–1770, 1240, and 1030–1200 $cm^{-1}$ in both AMP-W and FA+AMP-W samples. The 1510–1770 $cm^{-1}$ region encompasses contributions from lignin aromatic vibrations and carbonyl stretching bands; therefore, changes in this region cannot be solely attributed to phosphate-related vibrations. While phosphate-containing compounds may contribute to absorptions in this range (Liu et al. 2018; Xie et al. 2024), significant band overlap with inherent wood components limits definitive assignment.

The peak near 1240 $cm^{-1}$ can be associated to P=O stretching (Feng et al. 2017; Liu et al. 2018), although this region may also overlap with C–O vibrations of wood polysaccharides. Similarly, the peaks between 1030 and 1200 $cm^{-1}$ may include contributions from P=O and P–O–C vibrations of ammonium phytate (Feng et al. 2017; Fang et al. 2022), but this region strongly overlaps with C–O stretching vibrations of cellulose and hemicellulose. Therefore, these bands are interpreted as supportive evidence of AMP incorporation rather than conclusive proof of specific phosphate–wood covalent bond formation.

Moreover, characteristic absorption bands at 3220 and 1400 $cm^{-1}$ were detected in AMP-W and FA+AMP-W, corresponding to the stretching and bending vibrations of $NH_4^+$ ions (Liu et al. 2018; Xie et al. 2024). The absence of clearly distinguishable $NH_4^+$ bands in some spectra may result from overlap with the strong, broad O–H and C–H vibrations intrinsic to the wood matrix.

Overall, the FTIR results confirm chemical modification and the presence of phosphorus-containing species in the treated samples. Nevertheless, due to intrinsic band overlap and the qualitative nature of FTIR analysis, definitive conclusions regarding specific bonding configurations require complementary analytical techniques.

### 3.3 Scanning electron microscopy

Scanning electron microscopy (SEM) was used to examine the microstructural changes in poplar wood after treatment with ammonium phytate (AMP), furfuryl alcohol (FA), and their combination (FA+AMP), as presented in Fig. 3.

The raw wood (RW) exhibited a typical porous structure with clearly visible vessels, fibres, and interconnected voids (Fig. 3a, e). The lumina were open and no deposits were observed, confirming the untreated morphology of the wood.

After impregnation with AMP (AMP-W), the overall anatomical structure remained preserved (Fig. 2b, f). Compared to RW, the porous network appeared less open, indicating partial densification of the wood matrix. In addition, non-uniform deposits were observed within lumina and intercellular regions. These features may result from both AMP deposition and structural densification occurring during drying. Although SEM images alone cannot fully distinguish between these effects, SEM–EDX analysis confirmed the successful incorporation of AMP in the wood, as nitrogen and phosphorus were clearly detected in AMP-W (Table 4). The AMP-W sample contained 1.68% N and 0.66% P, verifying the presence of the nitrogen–phosphorus flame-retardant system within the treated wood. Such nitrogen-phosphorus incorporation is consistent with previous work using ammonium phytate and related phosphates as flame retardants for lignocellulosic materials (e.g., Feng et al. 2017; Zhang et al. 2023), where elemental analysis similarly confirmed N and P introduction.

In contrast, FA-treated wood (FA-W) showed a markedly different morphology compared to both RW and AMP-W. SEM images revealed pronounced filling of lumina and partial coverage of internal surfaces with a resin-like phase (Fig. 3c, g), characteristic of in situ polymerization of FA into poly(furfuryl alcohol) (PFA) under acidic conditions (Kong et al. 2018; Esteves and Pereira 2008). This polymerized phase formed within the porous structure and adhered to cell walls, explaining the high retention of FA after leaching and its contribution to dimensional stability and durability (Shen et al. 2020).

The combined FA+AMP treatment (FA+AMP-W) produced the most uniform microstructural modification (Fig. 3d, h). The FA+AMP-W sample exhibited a more continuous matrix and fewer discrete deposits, indicating that AMP was immobilized within the PFA network rather than present as loosely deposited particles. SEM–EDX confirmed that FA+AMP-W contained both N (2.11%) and P (0.71%), at levels comparable to AMP-W, demonstrating that the presence of furfurylation did not inhibit AMP incorporation.

To visualize elemental distribution, elemental mapping was conducted for the FA+AMP-W sample (Fig. 4). Maps of carbon (C), oxygen (O), and phosphorus (P) show that P is distributed across the analysed cross-sectional region rather than localized in isolated clusters. This relatively homogeneous P distribution supports the SEM observations and indicates that phosphorus-containing flame-retardant species are dispersed throughout the wood matrix. Mapping evidence of distributed flame-retardant elements has likewise been reported in studies where polymer networks were used to fix phosphate or phosphonate flame retardants in cellulosic substrates (Lin et al. 2021a; Kong et al. 2018).

Together with FTIR phosphate-related bands, these results support efficient immobilization of AMP in the modified wood. The fixation is most plausibly governed by a combination of physical encapsulation by PFA and strong ionic/hydrogen-bonding interactions; however, covalent

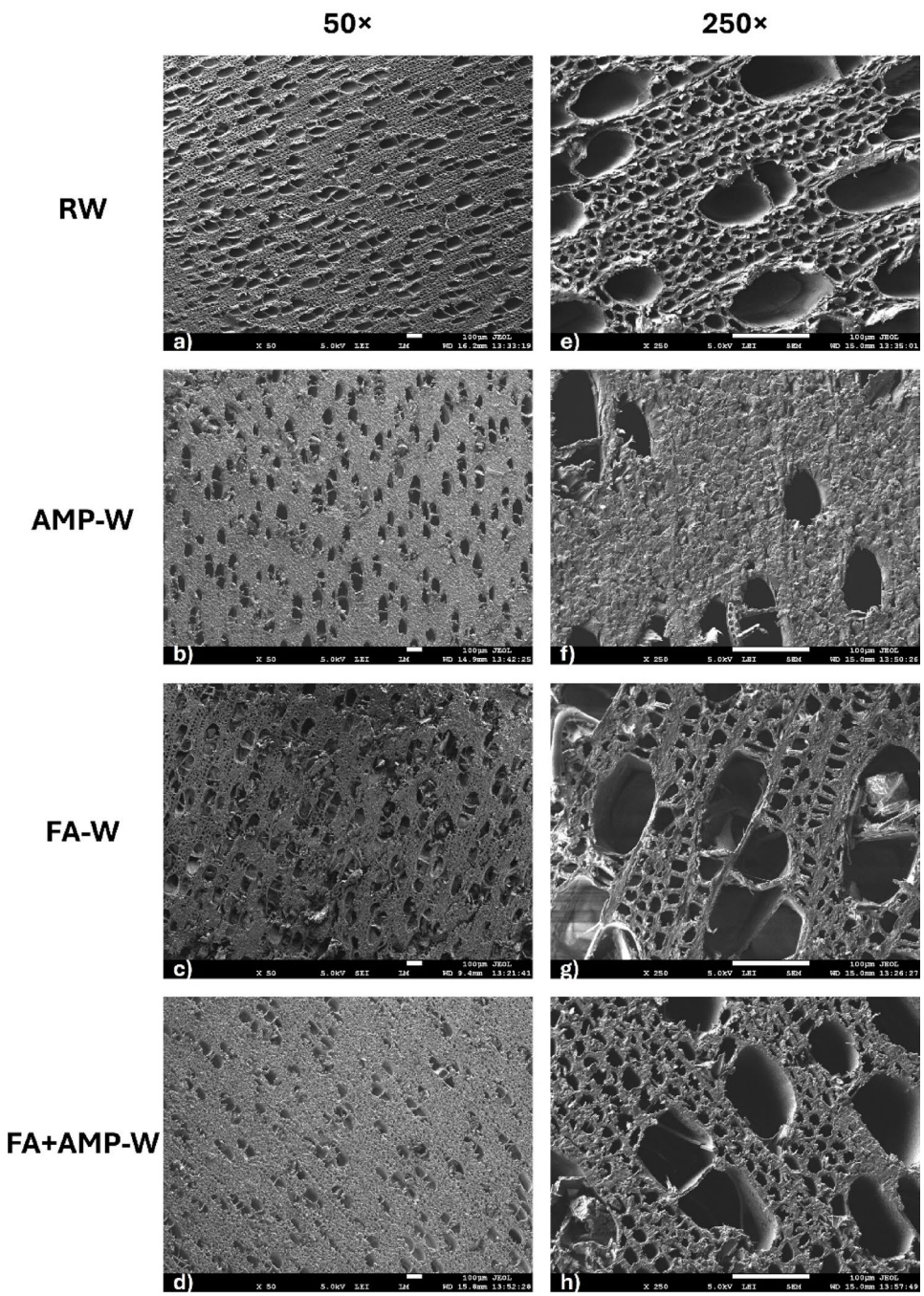


**Fig. 3** Scanning electron micrographs (SEM) images of the prepared wood samples in cross-section. The images show the surface morphology of: (**a**, **e**) raw wood (RW); (**b**, **f**) AMP-treated wood (AMP-W); (**c**, **g**) furfuryl alcohol-treated wood (FA-W); and (**d**, **h**) furfuryl alcohol and ammonium phytate-treated wood (FA+AMP-W). Figures a – d captured at 50× magnification; e – h captured at 250× magnification

**Table 4** Elemental composition (wt%) of raw wood and modified wood samples determined by SEM–EDX (normalized to 100%). n.d. = not detected

| | RW | FA-W | AMP-W | FA+AMP-W |
|---|---|---|---|---|
| C | 36.85% | 53.90% | 49.26% | 52.55% |
| O | 63.15% | 46.10% | 48.40% | 44.63% |
| N | n.d. | n.d. | 1.68% | 2.11% |
| P | n.d. | n.d. | 0.66% | 0.71% |
| Total | 100.00% | 100.00% | 100.00% | 100.00% |

RW: raw wood; FA-W: furfuryl alcohol-treated wood; AMP-W: ammonium phytate-treated wood; FA + AMP-W: combined treatment; values are given as mean ± standard deviation ($n = 3$)

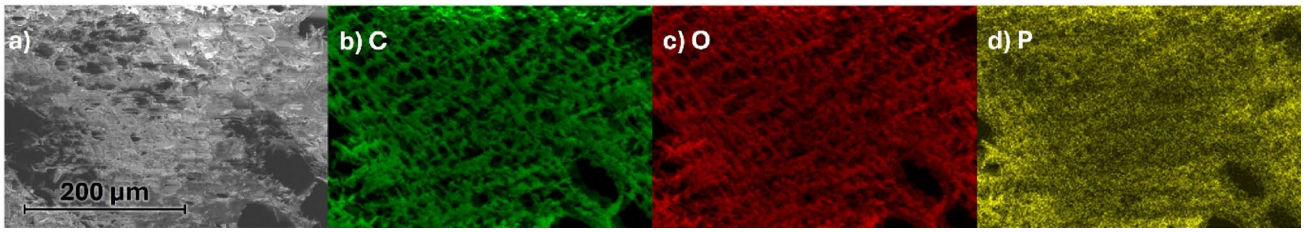


**Fig. 4** SEM–EDX elemental mapping of the FA+AMP-W sample: **a** SEM micrograph of the analysed cross-sectional area; **b** carbon (C) distribution map; **c** oxygen (O) distribution map; and **d** phosphorus (P) distribution map

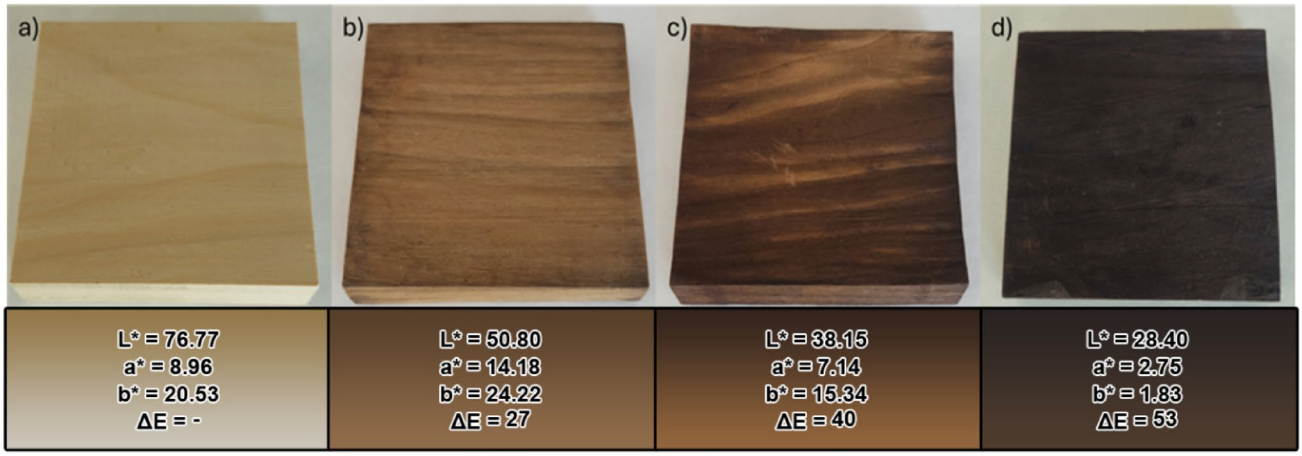


**Fig. 5** Photographs of wood samples: **a** raw wood (RW); **b** AMP-treated wood (AMP-W); **c** furfuryl alcohol-treated wood (FA-W); **d** furfuryl alcohol and AMP-treated wood (FA+AMP-W). The table below the images provides the CIELAB colour parameters for each sample: L∗ (lightness), a∗ (green-red axis), b∗ (blue-yellow axis), and ΔE (total colour difference). The ΔE values are calculated relative to the raw wood (RW) sample

bonding cannot be confirmed within the scope of the present characterization.

Overall, the combined SEM and SEM–EDX results provide direct evidence that the phosphoric-acid-catalysed in situ polymerization of FA promotes immobilization of AMP and enhances fixation of the nitrogen-phosphorus system within the wood structure. This structural and chemical integration explains the improved leach resistance and durable flame-retardant performance observed for FA+AMP-W, consistent with mechanistic insights into phosphorus-mediated char formation and gas-phase dilution effects reported in earlier flame-retardant wood studies (Hörold 2014; Qin et al. 2023).

## 3.4 Colour measurements

Colorimetric analysis using the CIELab model was performed to quantify colour changes and identify premium wood species with similar aesthetic qualities to the modified wood. Figure 5 demonstrates a progressive shift towards a yellowish-brown hue and increased darkening in the following order: AMP-W, FA+AMP-W, and FA-W. The pronounced colour change in FA-containing samples is consistent with in situ polymerization of furfuryl alcohol and formation of conjugated structures, which typically induce wood darkening. These changes may provide not only improved fire performance but also an aesthetically attractive appearance for high-value interior applications.

### 3.4.1 Hardness

The hardness of modified wood is critical for its intended applications and the results of both Shore D and Janka hardness measurements, are summarized in Fig. 6. The raw wood (RW) samples served as the baseline, and the reached values (50 Shore D – 50; Janka – 18 N mm$^{-2}$) are consistent with other works (Candan et al. 2013; Zhou et al. 2019). The AMP-W samples showed no significant change in Shore D and Janka hardness compared to RW. In contrast, the FA-W samples demonstrated a notable increase in both Shore D (7.1%) and Janka (18.0%) hardness. The most prevalent increase in Shore D hardness (12.2%) was observed for the FA+AMP-W samples. Janka hardness reached similar values as FA-W (18%). The incorporation of FA significantly improves the hardness of wood, as evidenced by the increase in both Shore D and Janka hardness values. However, the

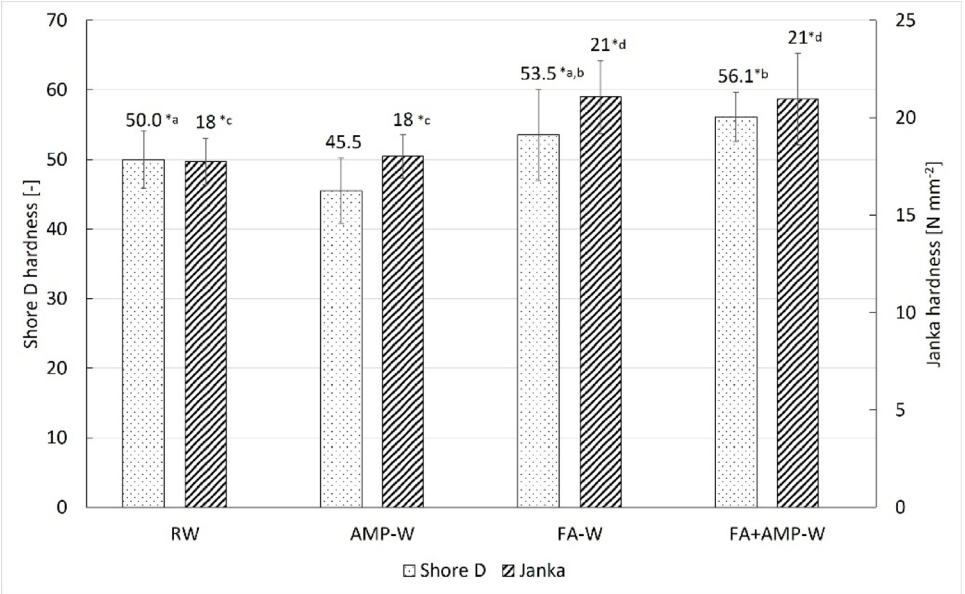


**Fig. 6** Shore D and Janka hardness of raw wood (RW); furfuryl alcohol-treated wood (FA-W); ammonium phytate-treated wood (AMP-W); and furfuryl alcohol and ammonium phytate-treated wood (FA+AMP-W). Superscript *a, *b, *c, and *d indicate that there is no statistically significant difference between the corresponding values (based on Duncan's multiple range test)

addition of AMP alone does not appear to have a significant impact on either Shore D or Janka hardness. The significantly higher Shore D hardness observed for FA+AMP-W compared to FA-W suggests that the presence of AMP contributes to increased resistance to localized indentation. This effect may be associated with additional rigid inorganic/phosphate-rich domains and stronger interfacial interactions within the furfurylated matrix, as supported by the confirmed presence and distribution of phosphorus in SEM–EDX analysis.

However, this contribution does not translate into a further increase in Janka hardness, indicating that the AMP-related reinforcement is more pronounced at the microscale surface response (Shore D) than in bulk resistance to deeper indentation.

## 3.5 Flexural strength

Flexural testing was performed to evaluate the bulk mechanical performance of the modified wood and to complement the hardness results presented in the previous section and was evaluated by three-point bending. Representative load–deflection curves are presented in Fig. 7. For clarity and direct comparison of failure behaviour, only the region close to the maximum load was plotted. Although RW exhibited progressive nonlinearity in the full load–deflection response, this region was excluded in order to focus on the deformation behaviour immediately preceding fracture. All samples showed an initial linear elastic response followed by deviation from linearity as damage accumulated.

The calculated modulus of rupture (MOR) and modulus of elasticity (MOE) values are summarized in Table 5. Raw wood (RW) exhibited MOR and MOE values of 76.0 ± 4.8 MPa and 8.57 ± 0.21 GPa, respectively. Furfurylation alone (FA-W) resulted in a slightly increased MOR (79.5 ± 1.5 MPa), while the MOE decreased to 7.61 ± 0.37 GPa. The AMP-treated sample (AMP-W) showed a MOR of 80.88 ± 5.2 MPa and a MOE of 8.37 ± 1.04 GPa, indicating that AMP impregnation alone did not negatively affect bending performance. This observation is consistent with the hardness results, where AMP-W exhibited no significant changes compared to RW.

In contrast, the combined FA+AMP treatment (FA+AMP-W) resulted in a pronounced reduction in bending performance. The MOR decreased to 47.0 ± 10.8 MPa and MOE to 6.67 ± 1.42 GPa, corresponding to approximately a 38% reduction in MOR relative to RW. The larger standard deviation observed for FA+AMP-W further suggests increased heterogeneity of the modified structure and/or variation in local defect distribution, which can strongly affect failure in bending.

The reduction in MOR and MOE for FA+AMP-W may appear inconsistent with the hardness results, where FA+AMP-W exhibited the highest Shore D hardness and Janka hardness comparable to FA-W. However, this behaviour reflects the different nature of these tests. Hardness measurements primarily assess localized resistance to indentation (surface and microscale stiffness), whereas bending performance depends on the integrity and toughness of the bulk structure and its ability to redistribute stresses without premature cracking.

The combined presence of polymerized FA and phosphate-nitrogen species from AMP likely increases local rigidity but also introduces brittleness and reduces strain-to-failure, leading to earlier fracture under flexural loading. Similar trade-offs between increased surface hardness

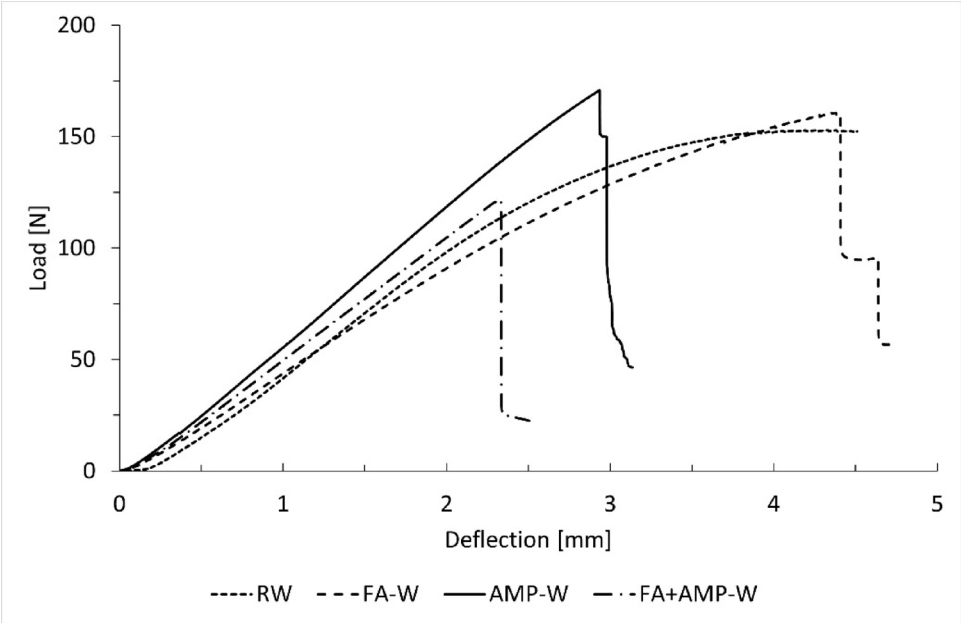


**Fig. 7** Load–deflection curves obtained from three-point bending tests of poplar wood samples: raw wood (RW), furfuryl alcohol–treated wood (FA-W), ammonium phytate–treated wood (AMP-W), and the combined FA+AMP treatment (FA+AMP-W)

**Table 5** Flexural properties of raw wood and modified wood samples determined by three-point bending (EN ISO 178)

| | MOR [MPa] | MOE [GPa] |
|---|---|---|
| RW | 76.0 ± 4.8 | 8.57 ± 0.21 |
| FA-W | 79.5 ± 1.5 | 7.61 ± 0.37 |
| AMP-W | 80.9 ± 5.2 | 8.37 ± 1.04 |
| FA+AMP-W | 47.0 ± 10.8 | 6.67 ± 1.42 |

RW: raw wood; FA-W: furfuryl alcohol-treated wood; AMP-W: ammonium phytate-treated wood; FA+AMP-W: combined treatment; values are given as mean ± standard deviation ($n = 6$)

and reduced flexural performance have been reported for chemically modified wood and phosphorus-treated systems, where increased crosslinking and stiffness reduce ductility and damage tolerance (Esteves and Pereira 2008; Hörold 2014; Qin et al. 2023).

Overall, while the FA–AMP system improves flame retardancy, leach resistance, and surface hardness, it reduces flexural strength and stiffness. This highlights the need to balance fire performance with mechanical integrity when designing durable multifunctional wood modification systems.

### 3.6 Water uptake and leaching test

The two-week water uptake (WU) measurements revealed a clear trend among the tested wood specimens (Fig. 8). The raw wood (RW) exhibited the highest water uptake at 170%. Treatment with ammonium phytate alone (AMP-W) resulted in a modest reduction to 157%, while treatment with furfuryl alcohol (FA-W) caused a more substantial decrease to 117%. The most effective treatment was the combination of furfuryl alcohol and ammonium phytate (FA+AMP-W), which showed the lowest water uptake at 106%, representing a significant improvement over the other treatments and a reduction of nearly 38% compared to the RW.

Water uptake analysis confirmed that furfuryl alcohol (FA) significantly enhances the dimensional stability of wood by reducing its hygroscopicity. This effect is attributed to the in-situ polymerization of FA within the cell wall, which fills nanopores and limits the availability of hydrophilic sorption sites (Thygesen et al. 2010; Sun et al. 2022). Ammonium phytate (AMP) alone showed only a minor reduction in water uptake; however, when combined with FA, a synergistic effect was observed. The FA+AMP-treated samples exhibited the lowest water uptake, suggesting improved moisture resistance due to combined polymer network formation and phosphate-based interactions.

This is supported by Xie et al. (2024), who demonstrated that poplar wood modified via in situ polymerization of FA and AMP exhibited exceptional water resistance and dimensional stability, alongside significantly improved flame retardant properties. These results indicate that dual modification with FA and AMP effectively enhances the wood's resistance to moisture, making it suitable for applications in humid or variable environments. Kong et al. (2018) demonstrated that combining furfuryl alcohol with ammonium dihydrogen phosphate (a simple inorganic phosphate) reduced water uptake and improved dimensional stability. While ammonium phytate differs structurally, its similar phosphorus content may lead to analogous synergistic effects when combined with FA, particularly in reducing wood hygroscopicity and improving water resistance.

Leach retention (LR) was used to assess the effectiveness of PFA and AMP fixation within the wood (Fig. 9). The

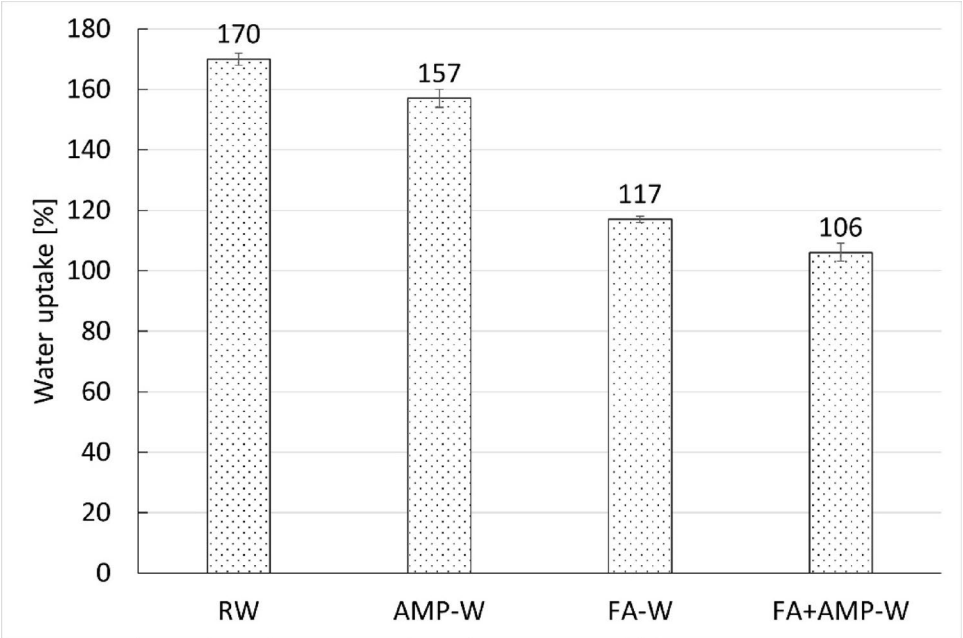


**Fig. 8** Two-week water uptake (WU) of raw wood (RW); furfuryl alcohol-treated wood (FA-W); ammonium phytate-treated wood (AMP-W); and furfuryl alcohol and ammonium phytate-treated wood (FA+AMP-W). All differences between the corresponding values are statistically significant (based on Duncan's multiple range test)

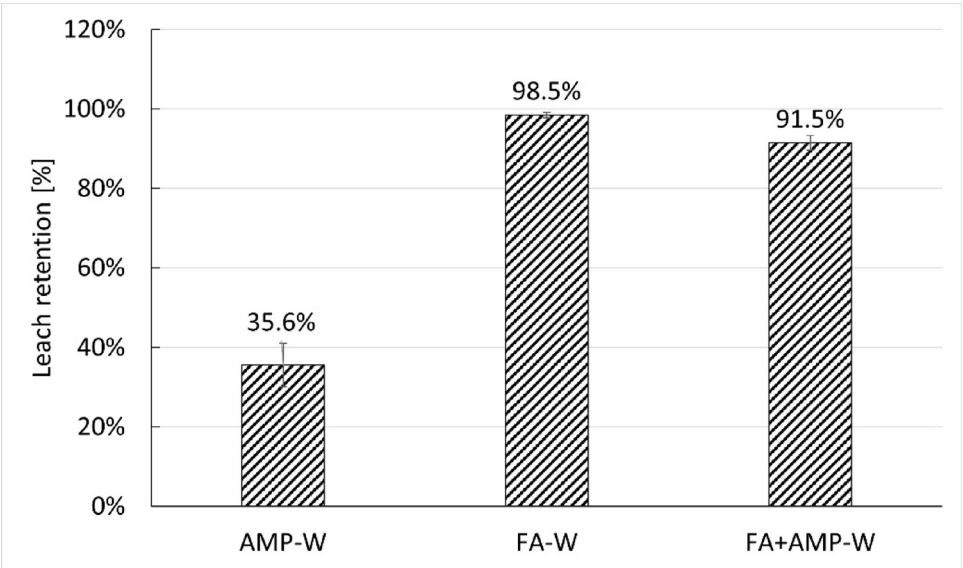


**Fig. 9** Leach retention of raw wood (RW); furfuryl alcohol-treated wood (FA-W); ammonium phytate-treated wood (AMP-W); and furfuryl alcohol and ammonium phytate-treated wood (FA+AMP-W). All differences between the corresponding values are statistically significant (based on Duncan's multiple range test)

results indicate that furfuryl alcohol (FA) plays a critical role in enhancing the retention and leaching resistance of water-based additives in modified poplar wood.

In the AMP-W sample, where only ammonium phytate (AMP) was used, leach retention was low (35.6%), indicating weak affinity between AMP and the wood matrix. This agrees with literature showing that phosphorus-based flame retardants readily leach when not fixed within a polymeric or crosslinked system, limiting their long-term effectiveness (Rowell 2012; Hörold 2014).

In contrast, FA-W samples exhibited near-complete retention (98.5%), reflecting effective in-situ polymerization of furfuryl alcohol within the cell walls. Acid-catalysed polymerization, promoted here by phosphoric acid, leads to formation of a crosslinked poly(furfuryl alcohol) (PFA) network that improves dimensional stability and fixation of the modifying agent (Mubarok et al. 2023; Iroegbu and Ray 2024).

The combined FA+AMP-W treatment achieved similarly high retention (91.5%), demonstrating that the PFA network effectively immobilizes AMP within the wood structure. This immobilization likely results from both physical entrapment within the polymer matrix and potential interactions between AMP and the polymerizing FA. A comparable effect was reported by Xie et al. (2024), where the combination of FA and AMP significantly improved retention compared to AMP alone.

The high retention observed in the present system is further supported by the use of phosphoric acid as a catalyst, which enables efficient FA polymerization while remaining in the wood as a non-volatile phosphorus source. Compared with stronger mineral acids, phosphoric acid provides effective catalysis while minimizing wood degradation (Zuo et al. 2023). The slight decrease in retention compared to FA alone could reflect either a minor disruption in FA polymerization due to the presence of AMP or partial leaching of AMP that was not fully immobilized.

Overall, these results demonstrate that acid-catalysed furfurylation substantially enhances the fixation of water-soluble flame retardants and that the FA–AMP–$H_3PO_4$ system provides a durable, multifunctional treatment combining high leach resistance with improved flame retardancy.

### 3.7 Thermal stability

To fully understand the flame-retardant mechanism of ammonium phytate (AMP) on wood, a thermogravimetric (TGA) analysis of the pure AMP material was first performed. This preliminary analysis allowed for the characterization of its thermal decomposition pathway and the identification of key degradation products, such as phosphoric acid, which is critical for its char-forming effect. Based on the thermogravimetric (TG) analysis, the decomposition of the prepared AMP occurs in four main stages, as shown in Fig. 10:

- Stage 1: Mass loss of approximately 3.5% occurs between 80 °C and 122 °C, with a maximum degradation rate observed at 114 °C.
- Stage 2: This is the most significant stage, occurring between 122 °C and 277 °C. The sample loses nearly 50% of its mass, with a peak in the derivative thermogravimetric (DTG) curve at 170 °C.
- Stage 3: Between 277 °C and 412 °C, the sample loses about 10% of its mass, and the maximum rate of mass loss is at 313 °C.
- Stage 4: A mass loss of 19% occurs in the temperature range of 412 °C to 615 °C, with the DTG peak occurring at 547 °C.

This decomposition profile is consistent with and expands upon findings in existing literature. Zhang et al. (2023) identified three main decomposition stages for AMP. They reported that the first stage (102 –232 °C) involves the decomposition of ammonium phytate and urea, releasing phosphoric acid and ammonia. While their subsequent two stages of decomposition were similar to those observed for phytic acid, their AMP analysis showed a broader DTG peak between 230 °C and 400 °C. They attributed this broader peak to secondary reactions of urea by-products. Similarly, Fang et al. (2022) stated that AMP decomposes to produce ammonia (at approximately 200 °C) and phosphate, which then decomposes to phosphoric acid. This formation of phosphoric acid is also supported by Feng et al. (2017), who further noted that some $-P-O-NH^{4+}$ groups remain in the charred residue of materials treated with AMP.

To evaluate the effectiveness of the treatments, thermogravimetric analysis (TGA) was conducted on all wood samples, comparing the thermal behaviour of the non-leached (Fig. 11) and leached (Fig. 12) samples. All the findings are presented in the Table 6.

The TG curves of the non-leached samples are shown in Fig. 11. All samples showed a minor initial mass loss on the TG curve at temperatures up to 115 °C. This phenomenon is commonly observed in lignocellulosic materials and is typically attributed to the evaporation of moisture (Li et al.

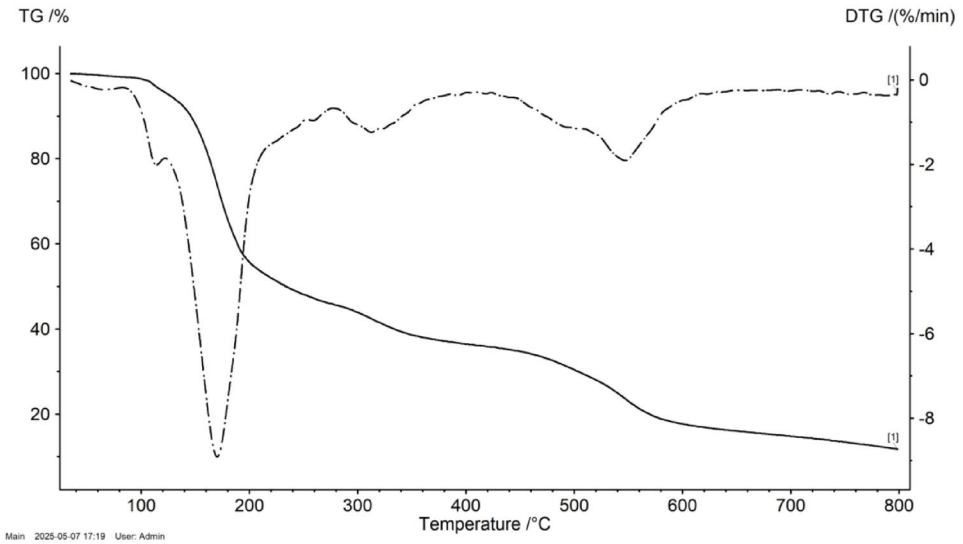


**Fig. 10** Thermogravimetric (TG) and derivative thermogravimetric (DTG) curves of ammonium phytate (AMP)

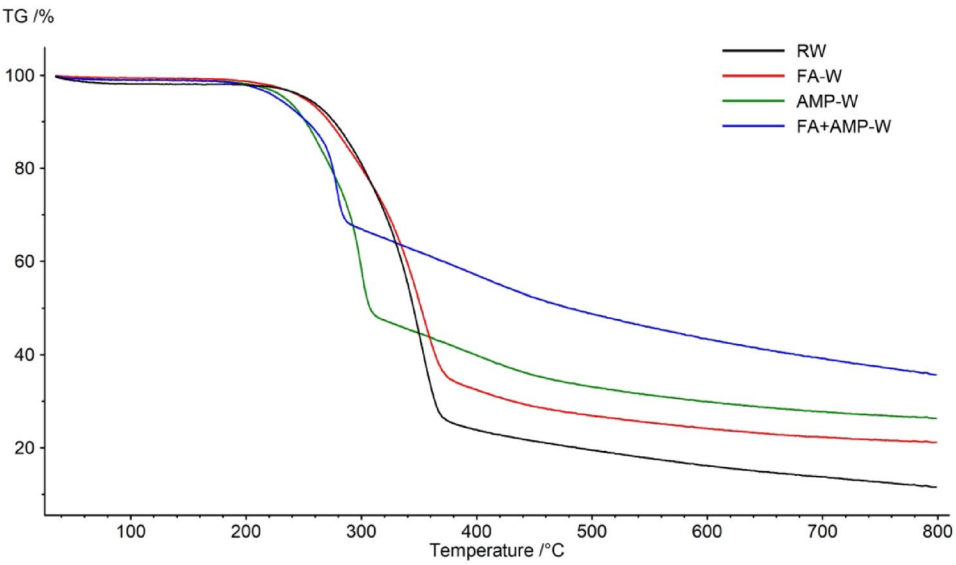


**Fig. 11** Thermogravimetric (TG) curves of the non-leached raw wood (RW); furfuryl alcohol-treated wood (FA-W); ammonium phytate-treated wood (AMP-W); furfuryl alcohol and ammonium phytate-treated wood (FA+AMP-W)

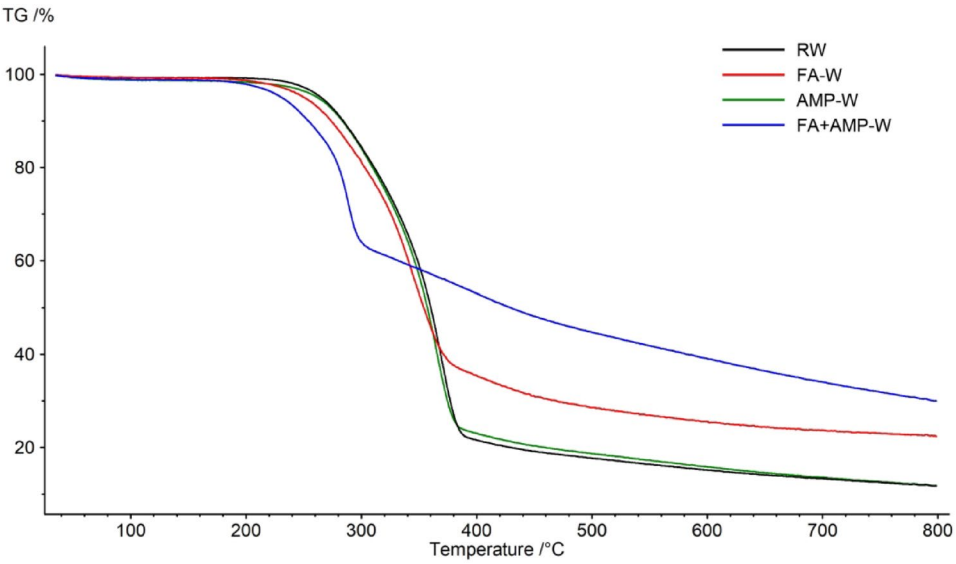


**Fig. 12** Thermogravimetric (TG) curves of the raw wood (RW); furfuryl alcohol-treated wood (FA-W); ammonium phytate-treated wood (AMP-W); furfuryl alcohol and ammonium phytate-treated wood (FA+AMP-W)

2019; Vahedi et al. 2022; Zhang et al. 2022a). Given that the materials were pre-dried at 103 °C before the analysis, this initial mass loss likely corresponds to moisture adsorbed during sample preparation.

In the second stage of mass loss, a significant difference is observed between samples containing AMP and those without it. The addition of AMP resulted in an acceleration of sample decomposition, shifting the DTG peak from approximately 350 °C to around 290 °C. Concurrently, the total mass loss was less pronounced, leading to a much higher char residue.

This phenomenon is caused by phosphoric acid, which redirects the thermal decomposition of cellulose. According to Zhang et al. (2023), the acid facilitates the production of a higher yield of char and less flammable gases at reduced temperatures.

The presence of furfuryl alcohol (FA) also had an evident impact, leading to a more significant formation of char residue. This outcome is consistent with prior work in the field, such as C. Lin et al. (2021a) and Acosta et al. (2022).

The TG curves for the leached samples (Fig. 12) show a very slight initial mass loss, similar to the non-leached samples, which is attributed to moisture removal. The progression of the TG curve for the raw wood (RW) sample is identical for both leached and non-leached wood.

However, a significant change is observed in the behaviour of the AMP-W sample, where its TG curve is practically identical to that of the RW sample. This suggests that almost all the AMP was leached out, as its effect on the thermal stability of the sample was no longer evident.

Conversely, the FA-W samples behaved nearly identically regardless of whether they were subjected to leaching.

**Table 6** Thermogravimetric analysis (TGA/DTG) parameters of raw wood (RW) and modified wood samples (FA-W, AMP-W, FA+AMP-W) before leaching (NL) and after water leaching (L). The first step corresponds to moisture release, while the second step represents the main thermal decomposition of wood polymers and/or modification products

| Sample | Leaching | 1st step | | | 2nd step | | | Residue at 800 °C [%] |
|---|---|---|---|---|---|---|---|---|
| | | Temperature range [°C] | $t_{pDTG}$ [°C] | Δm [%] | Temperature range [°C] | $t_{pDTG}$ [°C] | Δm [%] | |
| RW | NL | 35–115 | – | 1.6 | 203–385 | 352.2 | 73.1 | 11.6 |
| | L | 35–116 | – | 0.6 | 206–402 | 370.0 | 77.7 | 11.8 |
| FA–W | NL | 35–114 | – | 0.5 | 177–388 | 353.1 | 65.7 | 21.2 |
| | L | 35–90 | – | 0.6 | 181–407 | 344.4 | 64.4 | 22.4 |
| AMP–W | NL | 35–113 | – | 0.9 | 183–325 | 299.5 | 51.7 | 26.4 |
| | L | 35–115 | – | 1.1 | 178–398 | 365.2 | 75.4 | 11.9 |
| FA+AMP–W | NL | 35–92 | – | 0.8 | 159–296 | 278.4 | 31.5 | 35.7 |
| | L | 35–90 | – | 0.9 | 168–317 | 288.5 | 37.2 | 30.0 |

$t_{pDTG}$ – peak temperature of the derivative thermogravimetric (DTG) curve (maximum mass-loss rate); Δm – mass loss within the given temperature range; Residue at 800 °C corresponds to char yield at the end of the run; raw wood (RW); furfuryl alcohol-treated wood (FA-W); ammonium phytate-treated wood (AMP-W); furfuryl alcohol and ammonium phytate-treated wood (FA + AMP-W); NL-non-leached samples; L-leached samples

In the case of FA+AMP-W, only a minor change was observed after leaching. This indicates that a significant portion of the AMP was not removed, suggesting that the furfurylation process helped to prevent its leaching from the wood.

### 3.8 Fire performance test

Cone calorimetry was used for a comprehensive evaluation of the fire performance of raw and treated poplar wood, with results summarized in Table 7; Fig. 13. The analysis focused on comparing the performance between different sample types (RW, AMP-W, FA-W, and FA+AMP-W) and assessing the durability of the treatments by testing samples before (NL) and after (L) a rigorous 14-day leaching procedure. The statistical significance of investigated wood modification methods (both with and without leaching) on main fire performance parameters have been evaluated by the Duncan´s test at significance level $\alpha = 0.05$.

The time to ignition (TTI) was not significantly affected by any of the treatments, remaining consistent at approximately 7–8 s for most non-leached samples. This suggests the flame retardants act primarily during the combustion phase rather than delaying the initial ignition.

The raw wood samples served as a baseline for comparison. As expected, RW exhibited poor fire performance, characterized by a high MARHE of 172 kW $m^{-2}$ and a high THR of 129 MJ $m^{-2}$. The combustion process left a minimal RM of only 4.8%. The leaching process had a negligible impact on the fire performance of raw wood, with all key metrics remaining statistically similar after leaching.

Before leaching, the AMP-W samples showed a significant improvement in fire retardancy compared to RW. The MARHE was reduced by 28% to 124 kW $m^{-2}$, and the RM increased nearly four-fold to 18.5%. This demonstrates the effectiveness of AMP in promoting char formation. However, this protective effect was almost completely lost after leaching. The MARHE of the leached AMP-W sample rose to 155 kW $m^{-2}$, nearly reverting to the level of raw wood, and the RM dropped to 11.1%. This performance collapse is directly explained by the poor leach retention of AMP (only 35.6%), confirming that the flame retardant was washed out of the wood matrix. The thermogravimetric analysis (TGA) further supports this, showing the thermal decomposition curve of leached AMP-W is nearly identical to that of RW.

The FA treatment, both before and after leaching, did not significantly improve the primary fire performance indicators such as MARHE or $HRR_{max}$ compared to RW. However, it did notably increase the RM to 17.5% before leaching and 15.3% after, indicating that the polymerized FA network contributes to char formation. Crucially, the fire performance of FA-W was highly durable, with minimal changes to key metrics after the leaching process. This stability is attributed to the excellent leach retention of the in-situ polymerized FA (98.5%), which forms a stable, water-resistant matrix within the wood structure.

The combined FA+AMP (catalysed by $H_3PO_4$) treatment demonstrated a powerful synergistic effect, resulting in the best overall fire performance, which remained remarkably durable even after leaching. The non-leached FA+AMP-W samples showed outstanding fire retardancy. They achieved the lowest MARHE (120 kW $m^{-2}$) and THR (81 MJ $m^{-2}$) of all samples, representing a 30% and 37% reduction compared to RW, respectively. Most impressively, it produced the highest RM at 32.7%, a nearly seven-fold increase over RW, confirming a superior char-forming capability. The treatment was also highly effective at mitigating secondary fire hazards, significantly reducing TSP by 73% and COY by 22% compared to RW. While the leaching process slightly diminished its effectiveness, the leached FA+AMP-W

**Table 7** Cone calorimetry results of raw wood (RW) and modified wood samples before leaching (NL) and after leaching (L). Tests were performed according to ISO 5660-1 at a heat flux of 50 kW $m^{-2}$ (horizontal orientation). Values are reported as mean ± standard deviation ($n = 3$)

| Sample | RW | | AMP-W | | FA-W | | FA+AMP-W | |
|---|---|---|---|---|---|---|---|---|
| Leaching | NL | L | NL | L | NL | L | NL | L |
| TTI [s] | $7 \pm 1^{a)b)}$ | $7 \pm 1^{a)}$ | $7 \pm 1^{a)}$ | $7 \pm 2^{a)}$ | $7 \pm 1^{a)}$ | $10 \pm 2$ | $8 \pm 1^{b)c)}$ | $8 \pm 2^{b)c)}$ |
| $HRR_{max}$ [kW $m^{-2}$] | $172 \pm 5^{a)b)}$ | $174 \pm 10^{a)b)}$ | $124 \pm 11^{c)}$ | $155 \pm 4^{d)}$ | $179 \pm 10^{b)}$ | $178 \pm 4^{a)b)}$ | $120 \pm 12^{c)}$ | $151 \pm 8^{d)}$ |
| MARHE [kW $m^{-2}$] | $287 \pm 41^{a)}$ | $267 \pm 9^{b)}$ | $199 \pm 20^{c)}$ | $256 \pm 12^{b)}$ | $282 \pm 30^{a)}$ | $296 \pm 7^{a)}$ | $198 \pm 14^{c)}$ | $267 \pm 20^{b)}$ |
| THR [MJ $m^{-2}$] | $129 \pm 4^{a)}$ | $133 \pm 6$ | $107 \pm 9$ | $115 \pm 2$ | $137 \pm 9$ | $129 \pm 1^{a)}$ | $81 \pm 4$ | $93 \pm 4$ |
| EHC [MJ $kg^{-1}$] | $15.9 \pm 0.6^{a)}$ | $16.0 \pm 0.3^{a)}$ | $14.4 \pm 1.4^{b)}$ | $14.6 \pm 0.4^{b)}$ | $16.0 \pm 1.2^{a)}$ | $14.7 \pm 0.2^{b)}$ | $10.7 \pm 0.7$ | $12.3 \pm 0.5$ |
| RM [%] | $4.8 \pm 1.1^{a)}$ | $4.5 \pm 0.4^{a)}$ | $18.5 \pm 1.2$ | $11.1 \pm 1.2$ | $17.5 \pm 1.5$ | $15.3 \pm 0.8$ | $32.7 \pm 0.7$ | $30.6 \pm 0.3$ |
| TSP [$m^2$ $m^{-2}$] | $793 \pm 17^{a)}$ | $740 \pm 35^{b)}$ | $350 \pm 79$ | $680 \pm 67^{c)}$ | $673 \pm 119^{c)}$ | $774 \pm 47^{a)b)}$ | $213 \pm 42^{d)}$ | $209 \pm 26^{d)}$ |
| TCOP [g $m^{-2}$] | $463 \pm 28$ | $391 \pm 30$ | $253 \pm 36^{a)}$ | $267 \pm 22^{a)}$ | $272 \pm 36^{a)}$ | $264 \pm 39^{a)}$ | $337 \pm 22$ | $315 \pm 41$ |
| COY [g $kg^{-1}$] | $57.1 \pm 4.0$ | $47.1 \pm 1.1$ | $34.0 \pm 5.4^{a)}$ | $33.9 \pm 2.4^{a)}$ | $31.7 \pm 3.9^{a)b)}$ | $30.1 \pm 4.2^{b)}$ | $44.5 \pm 3.7$ | $41.8 \pm 6.2$ |

TTI: time to ignition; MARHE: maximum average rate of heat emission; $HRR_{max}$: maximum value of heat release rate during the test; THR: total heat release; EHC: effective heat of combustion; RM: residual mass; TSP: total smoke production; TCOP: total carbon monoxide production; COY: carbon monoxide yield;

Upper indexes a), b, c) and d) in one row indicate samples with no statistically significant difference values (Duncan´s test p value is higher than 0.05)

RW: raw wood; FA-W: furfuryl alcohol-treated wood; AMP-W: ammonium phytate-treated wood; FA + AMP-W: combined treatment; values are given as mean ± standard deviation ($n = 3$)

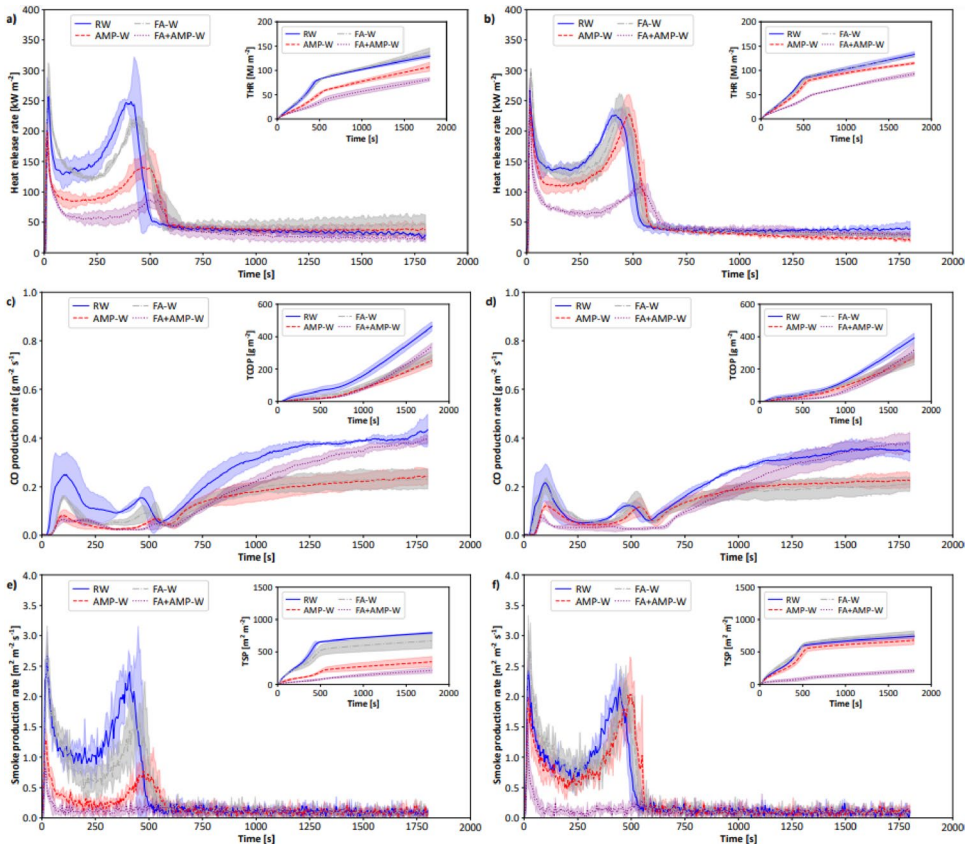


**Fig. 13** provides a dynamic visualization of the fire behaviour of the different wood samples over time, complementing the summary data in Table 7. The graphs for Heat Release Rate (HRR), Total Heat Release (THR), CO production and smoke production rates clearly demonstrate the superior and durable performance of the combined FA + AMP (catalysed by $H_3PO_4$) treatment as it creates a highly effective flame-retardant system. It excels at reducing the main fire hazards—heat, smoke, and toxic gases—and, most importantly, retains this high level of performance after being subjected to a rigorous leaching procedure

samples still significantly outperformed all other samples, including non-leached RW. Compared to the leached RW control, the leached FA+AMP-W sample achieved a 30% reduction in THR (from 133 to 93 MJ $m^{-2}$), a 13% reduction in the MARHE, a 72% reduction in TSP, and a nearly sevenfold increase in RM, from 4.5% to over 30.6%.

The notable reduction in TSP and COY can be attributed to the synergistic condensed- and gas-phase flame-retardant mechanisms introduced by the phosphate/nitrogen system. Phosphoric acid species promote dehydration and carbonization of cellulose, yielding a stable and cohesive char layer that inhibits the release of volatile combustibles and soot precursors, thereby lowering smoke formation in the condensed phase. Concurrently, the thermal decomposition of ammonium-based moieties generates non-flammable gases ($NH_3$ and $H_2O$), which dilute combustible pyrolysis vapours and quench flame-propagating radicals in the gas phase, leading to more complete combustion and correspondingly lower CO and smoke yields. Similar dual-mechanism suppression of heat release and smoke emission has been reported for phosphorylated polysaccharides and bio-based intumescent flame-retardant systems in wood and transparent-wood composites (Guo et al. 2025a, b; Fang et al. 2025).

Figure 13 Time-dependent fire performance of wood samples from cone calorimeter tests, comparing raw wood (RW), furfuryl alcohol-treated wood (FA-W), ammonium phytate-treated wood (AMP-W), and the combined treatment (FA+AMP-W). The figure shows: (a, b) Heat Release Rate (HRR) and inset Total Heat Release (THR); (c, d) Carbon Monoxide (CO) production rate and inset Total CO Production; and (e, f) Smoke production rate and inset Total Smoke Production (TSP). The left column (a, c, e) presents data for samples before leaching, while the right column (b, d, f) shows data after the leaching procedure. Solid lines depict the mean values, with the standard deviations represented by the shaded regions.

In this study, we classify a flame retardant as 'high-performance' based on a rigorous set of performance criteria that exceed standard benchmarks. To be designated as such, a system must demonstrate simultaneous improvement across all key fire performance indicators.

Furthermore, at least three of these key characteristics must show an improvement of at least 30%. In the case of our FA+AMP-W modification, these criteria were met by the RM, TSP, and TCOP parameters. While this is not a legally mandated definition, a thorough analysis of existing literature, e.g., (Lee et al. 2025) reveals that very few flame retardants can satisfy this complex combination of improvements simultaneously; thus, we consider them to be at the top of their category.

A particularly vital indicator is the Residual Mass (RM), which increased more than sixfold in our system. RM is a critical parameter for wood as it directly determines its fire resistance and ability to maintain structural integrity during combustion. The direct correlation between high RM and the fire resistance of wood composites has been confirmed in recent studies(Li et al. 2024b).

Even after leaching, FA+AMP-W maintained a high flame-retardant efficiency, characterized by a high limiting oxygen index (28%), significantly reduced peak heat release rate and total heat release, and low smoke production, which are comparable to the performance of state-of-the-art phosphorus–nitrogen flame-retardant wood systems (Lee et al. 2025). This exceptional durability is a direct result of the furfuryl alcohol polymer matrix effectively entrapping and fixing the AMP flame retardant within the wood, as evidenced by the high leach retention of 91.5%. The synergistic mechanism involves AMP's nitrogen-phosphorus action promoting a dense, insulating char layer (Qin et al. 2023), while the stable FA network ensures the flame retardant remains in place to function effectively, even after prolonged water exposure (Lin et al. 2021b). This combined action is the key to creating a durable, high-performance, flame-retardant lignocellulosic material. The main flame-retardant effect of phosphoric acid is the support of char layer formation (Kim and Kim 2025).

### 3.9 Limiting oxygen index

Raw wood (RW) exhibits the lowest LOI value at 18%, which is typical for untreated lignocellulosic materials and indicates high flammability. Treatment with ammonium phytate alone (AMP-W) increases the LOI to 26%, reflecting the known flame-retardant effect of phosphorus-based additives. Ammonium phytate functions primarily through a condensed-phase mechanism, promoting char formation and reducing the release of flammable volatiles during combustion (Qin et al. 2023).

In contrast, furfuryl alcohol treatment alone (FA-W) leads to a modest LOI increase to 21%. Although FA does not act as a flame retardant per se, its polymerization within the wood cell walls results in a denser, more thermally stable structure, which likely slows degradation and ignition. This moderate increase supports the idea that FA contributes indirectly to fire resistance through structural modification and enhanced thermal insulation (Esteves and Pereira 2008).

The highest LOI (28%) is observed for the combined FA+AMP-W treatment, indicating a clear synergistic effect between furfuryl alcohol and ammonium phytate. The improved retention of AMP due to the presence of FA (as shown previously) ensures that the phosphorus-based flame retardant remains in the matrix during combustion.

Simultaneously, the furfurylated structure enhances the thermal stability and promotes char formation. Together, these effects suppress flaming combustion and increase the oxygen concentration required to sustain burning. Such synergistic improvements are consistent with other studies where the incorporation of phosphorus compounds within crosslinked polymer matrices significantly boosts flame-retardant efficacy (Lin et al. 2021a; Ni et al. 2024).The Limiting Oxygen Index (LOI) results presented in Fig. 14. demonstrate significant improvements in flame retardancy as a result of chemical modification.

### 3.10 Flame test

To evaluate the flame retardancy of the modified wood samples, a propane torch flame test was conducted. The ignition behaviour and subsequent combustion characteristics were documented (Fig. 15). When subjected to the flame, raw wood (RW) demonstrated immediate ignition and rapid flame spread. Following a 10-second exposure, the entire wood block underwent vigorous combustion, culminating in complete burning within 65 s.

Unlike the rapid ignition and continuous burning seen in RW, AMP treated wood (AMP-W) showed a clear decrease in flame size after being exposed to a flame for 10 s, and it stopped burning on its own within another 37 s. This improved resistance to fire results from a combination of processes happening in both the gas and solid phases. When burning, AMP breaks down due to heat, releasing gases that don't burn, like ammonia and water vapor, which reduce the amount of oxygen available, thus suppressing the fire. Additionally, the volatile products produced during this breakdown include small molecules that act as scavengers of free radicals, interrupting the chemical reactions that keep a flame going. At the same time, the phosphoric acid that is released as AMP decomposes acts as a dehydrating agent, helping to form a protective layer of char from the wood's components and the PFA. The nitrogen contained within AMP also plays a role in building this dense char layer, which further enhances the material's ability to resist fire.

The furfuryl alcohol treated wood (FA-W) exhibited similar characteristic behaviour to RW. After removing the test flame the whole wood surface was engulfed with flames accompanied by a significant crackling and pieces of wood flying off the samples. While complete combustion occurred within 79 s, the FA-treated wood yielded a substantially greater amount of residual char compared to untreated wood.

Unlike the previous observations, or the FA+AMP-treated wood, self-extinguishment occurred remarkably quickly, within 9 s after the flame removal. This rapid response highlights the synergistic flame-retardant effect between AMP and polymerized FA. AMP, through its nitrogen-phosphorus intumescent mechanism, and FA, by promoting char formation, work together to create a dense char layer. By creating a barrier, this layer limits heat transfer, the release of combustible gases, and the entry of oxygen. As a result, it drastically lowers the intensity of combustion and emissions. The combined action of these components substantially enhances the wood's flame retardancy.

While previous studies have investigated furfuryl alcohol (FA) in combination with phosphorus-based flame retardants, the present work advances this concept in several critical ways. Kong et al. (2018) demonstrated improvements in dimensional stability and fire performance of poplar by combining FA with ammonium dihydrogen phosphate; however, the high loading levels and the inorganic phosphate used resulted in limited leach resistance. More recently, Xie et al. (2024) reported the use of FA with ammonium phytate (AMP), yet their system required higher concentrations of reagents and did not fully address the durability of flame-retardant performance after leaching. As summarized in Table 8, the FA–AMP system of

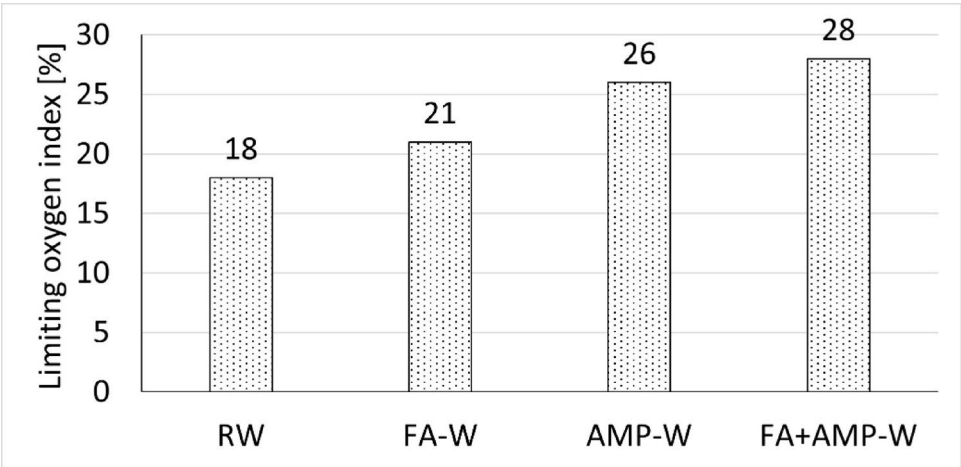


**Fig. 14** Limiting Oxygen Index (LOI) of raw wood (RW); ammonium phytate-treated wood (AMP-W); furfuryl alcohol-treated wood (FA-W); and furfuryl alcohol and ammonium phytate-treated wood (FA+AMP-W). Duncan's Multiple Range Test is not applicable to LOI data due to the threshold-based nature of the LOI measurement

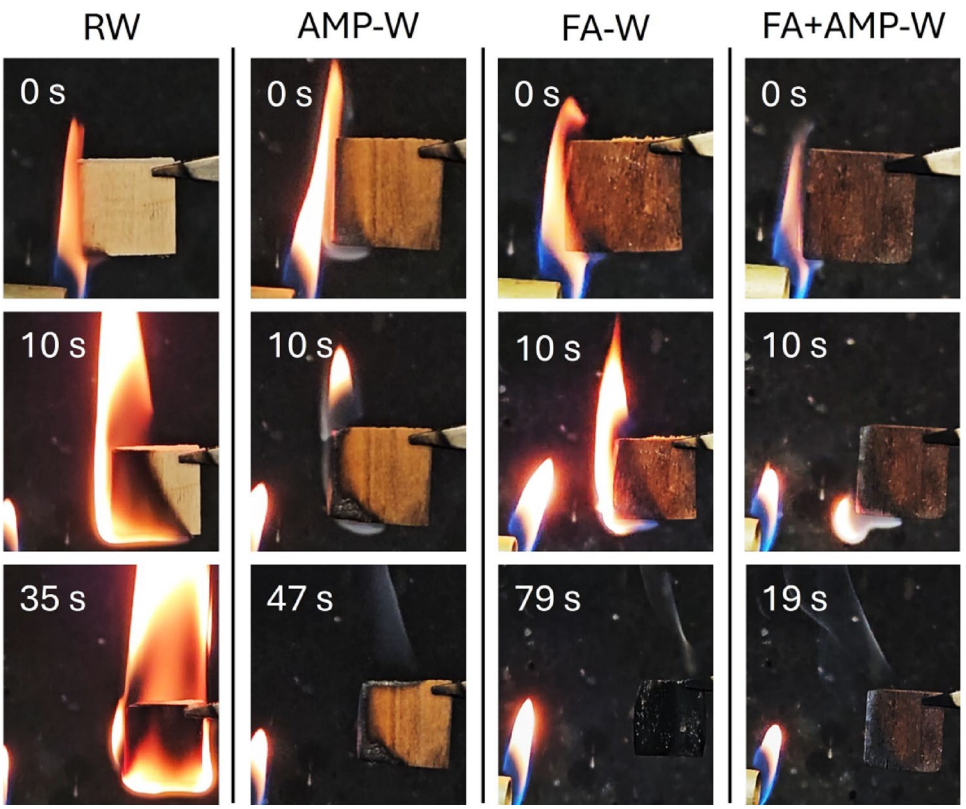


**Fig. 15** Flame test progression of various wood samples. The rows display the temporal stages of the test: 0 s (test flame application), 10 s (test flame removal), and flame extinction (except RW, where a fully developed flame is displayed). The columns correspond to the following wood treatments: raw wood (RW); ammonium phytate-treated wood (AMP-W); furfuryl alcohol-treated wood (FA-W); furfuryl alcohol and ammonium phytate-treated wood (FA+AMP-W)

**Table 8** Quantitative comparison of furfuryl alcohol (FA)-based flame-retardant wood modification systems reported in recent literature, including formulation, catalyst type, weight% gain (WPG), limiting oxygen index (LOI), total heat release reduction (THR ↓), and leaching retention

| FA [wt%] | Fire retardant [wt%] | Catalyst [wt%] | WPG [%] | LOI [%] | THR ↓ [%] | Leach retention [%] | Ref. |
|---|---|---|---|---|---|---|---|
| 20 | 8 AMP | 1.5 MA | ≈31 | ≈36 | ≈49 | ≈40 | (Xie et al. 2024) |
| 15 | 0.8 ADP | 3.2 BA | ≈23 | ≈34 | ≈37 | n.d. | (Zhang et al. 2022b) |
| 30 | 5 GUP | 3 MA, 1 TEA | ≈28 | ≈46 | n.d. | partial leaching | (Lin et al. 2021b) |
| 30 | 5 ADP | 2 MA | ≈68 | n.d. | ≈34 | ≈57 | (Kong et al. 2018) |
| 18 | 10 APP | 2 MA | ≈36 | ≈48 | ≈46 | ≈82 | (Yi et al. 2023) |
| 15 | 4 AMP | 0.16 PA | ≈22 | ≈28* | ≈37* | ≈92 | This study |

ADP: ammonium dihydrogen phosphate; AMP: ammonium phytate; APP: ammonium polyphosphate; BA: boric acid; GUP: guanyl-urea phosphate; FA: furfuryl alcohol; MA: maleic anhydride; PA: phosphoric acid; TEA: triethanolamine; n.d.: no data available;

WPG: weight% gain; LOI: limiting oxygen system; THR↓: Total heat release decrement [%]

* dry basis

Xie et al. (2024) achieved a high LOI (≈36%) and strong THR reduction (≈49%), but required 20 wt% FA and 8 wt% AMP, resulting in a higher WPG (≈31%) and only≈40% leach retention. In contrast, the present study employs lower concentrations of both FA (15 wt%) and AMP (4 wt%) and achieves a comparable THR reduction (≈37%) with a moderate WPG (≈22%). Importantly, the leaching retention of the present system (≈92%) exceeds that of most comparable FA-based flame-retardant systems reported in recent literature (Table 8), confirming efficient immobilization of the nitrogen–phosphorus flame retardant within the polymerized FA matrix. This improved durability is attributed to the use of phosphoric acid as a dual-function agent, which not only catalyses the in-situ polymerization of FA but also contributes additional phosphorus to promote dehydration and char formation. Moreover, unlike many previous studies that report fire performance only for non-leached samples, this work provides a systematic evaluation of flame-retardant performance both before and after leaching, demonstrating that the synergistic FA+AMP+$H_3PO_4$ system maintains high flame retardancy after water exposure.

Overall, the comparison confirms that the main practical contribution of this work is the development of a low-concentration, bio-based, and highly leach-resistant FA+AMP system catalysed by a small amount of phosphoric acid, which provides competitive fire performance while maximizing leach resistance.

## 4 Conclusion

A fully bio-based and durable flame-retardant modification system for poplar wood was developed using an in-situ polymerization approach combining furfuryl alcohol (FA) and ammonium phytate (AMP), catalysed by phosphoric acid. This treatment effectively immobilized AMP within the wood structure, resulting in a weight% gain of 21.7% and a leach resistance exceeding 91%, confirming efficient fixation of the flame-retardant components.

The FA+AMP-modified wood exhibited substantially improved fire performance. The limiting oxygen index increased from 18% to 28%, while cone calorimetry showed a 37% reduction in total heat release (from 129 to 81 MJ $m^{-2}$) and a 73% reduction in smoke production. In addition, the residual mass increased from 4.8% to 32.7%, demonstrating enhanced char formation. Direct flame tests further confirmed improved flame resistance, as FA+AMP-W self-extinguished within 9 s, whereas raw wood burned completely within 65 s. Importantly, the flame-retardant performance remained largely unchanged after water leaching, indicating excellent durability. The results suggest that the improved fire behaviour is governed by a combination of condensed-phase char promotion by phosphorus species and gas-phase dilution effects associated with nitrogen-containing components.

The mechanical evaluation showed that the modified wood retained satisfactory structural integrity. While FA incorporation increased hardness, the combined FA+AMP treatment caused a reduction in flexural strength, indicating a trade-off between improved fire safety and bulk mechanical performance. Nevertheless, the overall multifunctional behaviour of FA+AMP-W demonstrates a promising balance between durability, flame retardancy, and practical usability for interior and semi-structural applications.

Future work should focus on long-term performance under realistic service conditions, including cyclic humidity, temperature variations, ultraviolet exposure, and biological ageing. In addition, optimization of the impregnation and curing process is required to improve scalability, reduce energy and chemical consumption, and ensure consistent quality. Comprehensive life-cycle assessment and cost–performance analysis will also be necessary to evaluate industrial feasibility. Overall, the proposed FA+AMP system provides an environmentally friendly pathway for upgrading low-cost poplar wood into a fire-safe and durable material with potential for construction, furniture, and interior applications.

**Supplementary Information** The online version contains supplementary material available at https://doi.org/10.1007/s00107-026-02406-4.

**Author contributions** I.W.: Conceptualization, methodology, investigation, writing—original draft preparation, funding acquisition, supervision, project administrationV.K.: Data curation, formal analysis, and visualizationT.Š.: Writing—review and editing, formal analysis, visualizationP.R.: Validation, experimental design support, data analysisJ.M.: software, data analysisC.-F.L.: Conceptualization, methodologyL.B.: Investigation, data analysisAll authors read and approved the final manuscript.

**Funding** Open access funding provided by The Ministry of Education, Science, Research and Sport of the Slovak Republic in cooperation with Centre for Scientific and Technical Information of the Slovak Republic. Funded by the EU NextGenerationEU through the Recovery and Resilience Plan for Slovakia under the project No. 09I03-03-V04-00459.

**Data availability** No datasets were generated or analysed during the current study.

## Declarations

**Conflict of interest** The authors declare no competing interests.



## References

Abou-Okeil A, El-Sawy SM, Abdel-Mohdy FA (2013) Flame retardant cotton fabrics treated with organophosphorus polymer. Carbohydr Polym 92:2293–2298. https://doi.org/10.1016/j.carbpol.2012.12.008

Acosta AP, Beltrame R, Missio AL et al (2022) Juvenile and mature woods from pine subjected to in situ polymerization with furfuryl alcohol. Wood Mater Sci Eng 17:151–156. https://doi.org/10.1080/17480272.2020.1810118

ASTM International (2022) Standard Test Methods for Small Clear Specimens of Timber. ASTM D143-22

Brisebois P, Aouinti M, Jafari M et al (2025) Adsorption Dynamics of Disodium Octaborate Tetrahydrate on Clay Minerals: Implications for Construction Wood Protection. Small Methods 9:2400753. https://doi.org/10.1002/smtd.202400753

Candan Z, Korkut S, Unsal O (2013) Thermally Compressed Poplar Wood (TCW): Physical and Mechanical Properties. Drv Ind 64:107–111. https://doi.org/10.5552/drind.2013.1216

Cheng X-W, Guan J-P, Tang R-C, Liu K-Q (2016) Phytic acid as a bio-based phosphorus flame retardant for poly(lactic acid) nonwoven fabric. J Clean Prod 124:114–119. https://doi.org/10.1016/j.jclepro.2016.02.113

Choura M, Belgacem NM, Gandini A (1996) Acid-Catalyzed Polycondensation of Furfuryl Alcohol: Mechanisms of Chromophore

Formation and Cross-Linking. Macromolecules 29:3839–3850. https://doi.org/10.1021/ma951522f
Dong Y, Xue Q, Fu Z et al (2023) Enhancing wood stability and fire retardancy through citric acid and phosphorylated sucrose stearate cross-linking modification. Constr Build Mater 393:131946. https://doi.org/10.1016/j.conbuildmat.2023.131946
Ehmcke G, Koch G, Richter K, Pilgård A (2020) Topochemical and light microscopic investigations of non-enzymatic oxidative changes at the initial decay stage of furfuryl alcohol-modified radiata pine (Pinus radiata) degraded by the brown rot fungus Rhodonia placenta. Int Biodeterior Biodegradation 154:105020. https://doi.org/10.1016/j.ibiod.2020.105020
Esteves BM, Pereira HM (2008) Wood modification by heat treatment: A review. BioResources 4:370–404. https://doi.org/10.15376/biores.4.1.Esteves
European Committee for Standardization (2020) Wood preservatives — Accelerated ageing of treated wood prior to biological testing — Leaching procedure. EN 842020
Fang Y, Chen K, Xu L et al (2025) Advances in Wood Processing, Flame-Retardant Functionalization, and Multifunctional Applications. Polym (Basel) 17:2677. https://doi.org/10.3390/polym17192677
Fang Y, Wu J, Sun W, Liu X (2022) Pyrolysis of Precious Chinese Xuan Paper Containing Ammonium Phytate as a Flame Retardant. ACS Omega 7:37971–37979. https://doi.org/10.1021/acsomega.2c05138
Feng Y, Zhou Y, Li D et al (2017) A plant-based reactive ammonium phytate for use as a flame-retardant for cotton fabric. Carbohydr Polym 175:636–644. https://doi.org/10.1016/j.carbpol.2017.06.129
Gaefke CB, Botelho EC, Ferreira NG, Rezende MC (2007) Effect of furfuryl alcohol addition on the cure of furfuryl alcohol resin used in the glassy carbon manufacture. J Appl Polym Sci 106:2274–2281. https://doi.org/10.1002/app.26938
Gao Y-Y, Deng C, Du Y-Y et al (2019) A novel bio-based flame retardant for polypropylene from phytic acid. Polym Degrad Stab 161:298–308. https://doi.org/10.1016/j.polymdegradstab.2019.02.005
Grdadolnik J, Maréchal Y (2002) Urea and urea-water solutions - An infrared study. J Mol Struct 615:177–189
Guo M, Pan Y, Xu S et al (2025a) Phosphorylated sodium alginate-filled delignified wood-reinforced transparent wood: Crafting flame-retardant composites. Carbohydr Polym 366:124021. https://doi.org/10.1016/j.carbpol.2025.124021
Guo M, Pan Y, Xu S et al (2025b) Sustainable, transparent and fire-retardant wood composites. Ind Crops Prod 233:121332. https://doi.org/10.1016/j.indcrop.2025.121332
Hill CAS (2006) Wood Modification. Wiley
Hörold S (2014) Phosphorus-based and Intumescent Flame Retardants. In: Papaspyrides CD, Kiliaris PBT-PGFR (eds) Polymer Green Flame Retardants. Elsevier, Amsterdam, pp 221–254
International Organization for Standardization (2015) ISO 5660-1:2015 Reaction-to-fire tests — Heat release, smoke production and mass loss rate — Part 1: Heat release rate (cone calorimeter method) and smoke production rate (dynamic measurement). 55
International Organization for Standardization (2017a) Plastics — Determination of burning behaviour by oxygen index — Part 2: Ambient-temperature test. ISO 4589–22017
International Organization for Standardization (2017b) Plastics — Determination of the burning behaviour by oxygen index — Part 2: Ambient-temperature test (ISO Standard No. 4589-2:2017)
International Organization for Standardization (2018) Rubber, vulcanized or thermoplastic — Determination of hardness — Part 4: Indentation hardness by durometer method (Shore hardness). ISO 48-42018
International Organization for Standardization (2019) Plastics — Determination of flexural properties. ISO 1782019
Iroegbu AOC, Ray SS (2024) On the chemistry of furfuryl alcohol polymerization: A review. J Polym Sci 62:1044–1060. https://doi.org/10.1002/pol.20230708
Jones D, Sandberg D, Goli G, Todaro L (2020) Wood Modification in Europe. Firenze University, Florence
Kim G, Kim D (2025) The Effect of Phosphoric Acid on the Flame Retardancy and Interfacial Adhesion of Carbon Fiber with Thermoplastic Resin PA6. Polym (Basel) 17:381. https://doi.org/10.3390/polym17030381
Kong L, Guan H, Wang X (2018) In Situ Polymerization of Furfuryl Alcohol with Ammonium Dihydrogen Phosphate in Poplar Wood for Improved Dimensional Stability and Flame Retardancy. ACS Sustain Chem Eng 6:3349–3357. https://doi.org/10.1021/acssuschemeng.7b03518
Lee YX, Wang W, Lei Y et al (2025) Flame-retardant coatings for wooden structures. Prog Org Coat 198:108903. https://doi.org/10.1016/j.porgcoat.2024.108903
Li H, Zheng Z, Liu Y et al (2024a) Construction of fully bio-based flame retardant and antibacterial coating on polyester fabric with chitosan and ammonium phytate. J Appl Polym Sci 141:e55940. https://doi.org/10.1002/app.55940
Li J, Jiang W, Liu M (2022) Durable phosphorus/nitrogen flame retardant for cotton fabric. Cellulose 29:4725–4751. https://doi.org/10.1007/s10570-022-04558-x
Li L, Yu L, Wu Z, Hu Y (2019) Delignification of poplar wood with lactic acid-based deep eutectic solvents. Wood Res 64:507–522
Lin C-F, Karlsson O, Martinka J et al (2021a) Approaching Highly Leaching-Resistant Fire-Retardant Wood by In Situ Polymerization with Melamine Formaldehyde Resin. ACS Omega 6:12733–12745. https://doi.org/10.1021/acsomega.1c01044
Lin C, Kim I, Mantanis GI et al (2021b) Leach-resistant fire-retardant treated furfurylated wood by incorporating guanyl-urea phosphate. Wood Mater Sci Eng 16:429–431. https://doi.org/10.1080/17480272.2021.1981998
Liu Q, Du H, Lyu W (2021) Physical and Mechanical Properties of Poplar Wood Modified by Glucose-Urea-Melamine Resin/Sodium Silicate Compound. Forests 12:127. https://doi.org/10.3390/f12020127
Liu X, Liu J, Dong Y et al (2022) Evaluation of natural weathering and thermal degradation behavior of furfurylated bamboo strips at different weight% gain. Eur J Wood Wood Prod 80:289–299. https://doi.org/10.1007/s00107-021-01784-1
Liu X, Zhang Q, Cheng B et al (2018) Durable flame retardant cellulosic fibers modified with novel, facile and efficient phytic acid-based finishing agent. Cellulose 25:799–811
Li X, Yue K, Zhu L et al (2024b) Relationships between wood properties and fire performance of glulam columns made from six wood species commonly used in China. Case Stud Therm Eng 54:104029. https://doi.org/10.1016/j.csite.2024.104029
Lowden LA, Hull TR (2013) Flammability behaviour of wood and a review of the methods for its reduction. Fire Sci Rev 2:4. https://doi.org/10.1186/2193-0414-2-4
Mubarok M, Azadeh E, Obounou Akong F et al (2023) Effect of Tannins Addition on Thermal Stability of Furfurylated Wood. Polym (Basel) 15:2044. https://doi.org/10.3390/polym15092044
Ni M, Li L, Wu Y et al (2024) Biobased Furfurylated Poplar Wood for Flame-Retardant Modification with Boric Acid and Ammonium Dihydrogen Phosphate. J Renew Mater 12:1355–1368. https://doi.org/10.32604/jrm.2024.054050
Origo FD, Arisseto JC, Seixas FL et al (2016) Acid catalyst influence on the polymerization time of polyfurfuryl alcohol and on the porosity of monolithic vitreous carbon. J Appl Polym Sci 133. https://doi.org/10.1002/app.43272

Page J, Whaley P, Bellingham M et al (2023) A new consensus on reconciling fire safety with environmental & health impacts of chemical flame retardants. Environ Int 173:107782. ttps://doi.org/https://doi.org/10.1016/j.envint.2023.107782

Qin S, Liu Y, Shi X et al (2023) Phytic acid-based NP fire retardant and its effect on combustion property of poplar wood. BioResources 19:955–972. https://doi.org/10.15376/biores.19.1.955-972

Rantuch P, Kvorková V, Wachter I et al (2024) Is biochar a suitable fire retardant for furfurylated wood? Compos Part. ttps://doi.org/10.1016/j.jcomc.2024.100454. C Open Access 14:

Rowell R (1983) Chemical Modification of Wood. Prod Abstr 6. ttps://doi.org/10.3139/9783446442504.022

Rowell R (2012) Handbook Of Wood Chemistry And Wood Composites, 2nd edn. CRC, Boca Raton

Sangregorio A, Muralidhara A, Guigo N et al (2020) Humin based resin for wood modification and property improvement. Green Chem 22:2786–2798. https://doi.org/10.1039/C9GC03620B

Shen X, Jiang P, Guo D, et al (2020) Effect of furfurylation on hierarchical porous structure of poplar wood. Polymers (Basel) 13:32

Song F, Liu T, Fan Q et al (2022) Sustainable, high-performance, flame-retardant waterborne wood coatings via phytic acid based green curing agent for melamine-urea-formaldehyde resin. Prog Org Coat 162:106597. ttps://doi.org/https://doi.org/10.1016/j.porgcoat.2021.106597

Sun H, Chang X, Fu C et al (2022) Effect of Impregnation with a Low-Concentration Furfuryl Alcohol Aqueous Solution on Hygroscopic Properties of Chinese Fir and Poplar Wood. Forests 13:1176. https://doi.org/10.3390/f13081176

Thygesen L, Thybring E, Hoffmeyer P (2010) Water sorption in wood and modified wood at high values of relative humidity. Part I: Results for untreated, acetylated, and furfurylated Norway spruce. Holzforschung 64:315–323. https://doi.org/10.1515/HF.2010.044

Vahedi N, Tiago C, Vassilopoulos AP et al (2022) Thermophysical properties of balsa wood used as core of sandwich composite bridge decks exposed to external fire. Constr Build Mater 329:127164. ttps://doi.org/https://doi.org/10.1016/j.conbuildmat.2022.127164

Wu M, Emmerich L, Kurkowiak K, Militz H (2023) Fire resistance of pine wood treated with phenol-formaldehyde resin and phosphate-based flame retardant. Wood Mater Sci Eng 18:1933–1939. https://doi.org/10.1080/17480272.2023.2205379

Xie K, Gao A, Zhang Y (2013) Flame retardant finishing of cotton fabric based on synergistic compounds containing boron and nitrogen. Carbohydr Polym 98:706–710. https://doi.org/10.1016/j.carbpol.2013.06.014

Xie S, Liu Z, Feng A et al (2024) Flame retardant modification of poplar wood based on sustainable impregnation solution with high biomass content. Ind Crops Prod 215:118616. https://doi.org/10.1016/j.indcrop.2024.118616

Yang T, Mei C, Ma E (2022a) Combined effects of multi-interfacial furfurylation and densification on mechanical-physical performances of fast-growing poplar wood. J Mater Sci 57:15340–15353. https://doi.org/10.1007/s10853-022-07581-2

Yang T, Zhang K, Mei C et al (2022b) Effects of furfurylation on interactions between moisture sorption and humidity conditioning of wood. Wood Sci Technol 56:703–720. https://doi.org/10.1007/s00226-022-01375-0

Yao M, Yang Y, Song J et al (2017) Lignin-based catalysts for Chinese fir furfurylation to improve dimensional stability and mechanical properties. Ind Crops Prod 107:38–44. ttps://doi.org/https://doi.org/10.1016/j.indcrop.2017.05.038

Yi X, Cao S, Hao X et al (2023) Dimensionally stable, flame-retardant, and leach-resistant furfurylated wood prepared by incorporating ammonium polyphosphate and nano-silica. Polym Adv Technol 34:2501–2514. https://doi.org/10.1002/pat.6067

Zhang L, Chen K, Xu B et al (2022a) Parallel-to-Grain Compressive and Tensile Behavior of Paulownia Wood at Elevated Temperatures. Appl Sci 12. ttps://doi.org/10.3390/app122312118

Zhang L, Xu J, Shen H et al (2021) Montmorillonite-catalyzed furfurylated wood for flame retardancy. Fire Saf J 121:103297. ttps://doi.org/https://doi.org/10.1016/j.firesaf.2021.103297

Zhang L, Zhang W, Peng Y et al (2022b) Thermal behavior and flame retardancy of poplar wood impregnated with furfuryl alcohol catalyzed by boron/phosphorus compound system. Ind Crops Prod 176:114361. ttps://doi.org/https://doi.org/10.1016/j.indcrop.2021.114361

Zhang S, Chen Z, Ding M et al (2020) Reducing the fire toxicity of wood composites using hierarchically porous 4A (H4A) zeolite modified ammonium polyphosphate (APP) synthesized by a facile in-situ method. Constr Build Mater 262:120754. ttps://doi.org/https://doi.org/10.1016/j.conbuildmat.2020.120754

Zhang S, Yang W, Yang T et al (2023) Thermal degradation, flame retardancy, and char analysis of ammonium phytate-based flame retardant treated loblolly pine wood. Eur J Wood Wood Prod 81:957–971. https://doi.org/10.1007/s00107-023-01927-6

Zhou Q, Chen C, Tu D et al (2019) Surface densification of poplar solid wood: Effects of the process parameters on the density profile and hardness. BioResources 14:4814–4831. https://doi.org/10.15376/biores.14.2.4814-4831

Zuo C, Guo Y, Jiang L et al (2023) Fabrication of durable flame retardant PAN fibers through bio-based ammonium phytate surface modification and highly efficient thermal oxidation. Eur Polym J 196:112304. ttps://doi.org/https://doi.org/10.1016/j.eurpolymj.2023.112304